


Review

Echocardiography in the Diagnosis and Management of Tricuspid Atresia

P. Syamasundar Rao 

McGovern Medical School, University of Texas-Houston, Children's Memorial Hermann Hospital, 6410 Fannin Street, UTPB Suite # 425, Houston, TX 77030, USA; P.Syamasundar.Rao@uth.tmc.edu or srao.patnana@yahoo.com; Tel.: +1-713-500-5738; Fax: +1-713-500-5751

Abstract: This review focuses on the utility of echocardiographic studies in the diagnosis of tricuspid atresia (TA) and in its management. Tricuspid atresia is a cyanotic congenital heart defect (CHD) accounting for nearly 1.5% of all CHDs. It is generally classified according to the morphology of the atretic tricuspid valve and associated heart defects. Following the description of the anatomic features of TA, echocardiographic features characteristic for TA were illustrated. Subsequent to a review of palliative and corrective procedures to treat TA, echocardiographic evaluation at each stage of Fontan was detailed. The role of echocardiography in the assessment of cardiac defects responsible for interstage mortality was also addressed. It was concluded that echo-Doppler studies are useful in the diagnosis and management of TA.

Keywords: echocardiography; Doppler; tricuspid atresia; patent foramen ovale; ventricular septal defect; pulmonary stenosis; transposition of the great arteries; coarctation of the aorta; Blalock–Taussig shunt; pulmonary artery banding; bidirectional Glenn; Fontan; interstage mortality



Citation: Rao, P.S. Echocardiography in the Diagnosis and Management of Tricuspid Atresia. *Appl. Sci.* **2021**, *11*, 9472. <https://doi.org/10.3390/app11209472>

Academic Editor: Qi-Huang Zheng

Received: 4 September 2021

Accepted: 8 October 2021

Published: 12 October 2021

Publisher's Note: MDPI stays neutral with regard to jurisdictional claims in published maps and institutional affiliations.



Copyright: © 2021 by the author. Licensee MDPI, Basel, Switzerland. This article is an open access article distributed under the terms and conditions of the Creative Commons Attribution (CC BY) license (<https://creativecommons.org/licenses/by/4.0/>).

1. Introduction

Tricuspid atresia (TA) is a cyanotic, congenital heart defect (CHD) and is defined as congenital absence or agenesis of the morphologic tricuspid valve [1–3]. It is the third most common cyanotic CHD, and is the most common cause of cyanosis with left ventricular hypertrophy. The prevalence of TA is estimated to be 2.9% of autopsy cases [4] and 1.4% to 1.5% of the clinical cases of CHD [4,5]. The main focus of this review is to present the role of echocardiography in the diagnosis and management of tricuspid atresia. Initially, the anatomic features of TA will be summarized, followed by a description of the historical aspects of the evolution of the echo of TA. Then, echo features, on the basis of current technology, both with respect to the diagnosis and management, will be reviewed.

2. Anatomic Features of TA

TA has been classified on the basis of valve morphology (Figure 1) [1,5,6], pulmonary vascular markings on chest roentgenogram [7], and associated cardiac defects (Figure 2) [1,8–11]. On the basis of the morphologic appearance of the atretic tricuspid valve, it has been characterized as muscular, membranous, valvular, Ebstein's, unguarded with muscular shelf, and atrioventricular canal types (Figure 1) [1,6,12]. The muscular type is the most common variety and constitutes 89% of all TA cases [1,12,13]; other types occur with much lower frequency, as shown in Figure 1. The classification based on associated cardiac defects largely centers on the interrelationship of the great arteries (Figure 2, top): Type I, normally related great arteries; Type II, d-transposition of the great arteries; Type III, malpositions of the great arteries other than d-transposition; and Type IV, truncus arteriosus. Each type is again divided into subgroups on the basis of the pulmonary artery anatomy (Figure 2, bottom): subgroups—a. pulmonary atresia, b. pulmonary stenosis or hypoplasia, and c. normal pulmonary arteries (no pulmonary stenosis). It is generally thought that classification based on associated cardiac defects is more useful clinically [1,13].

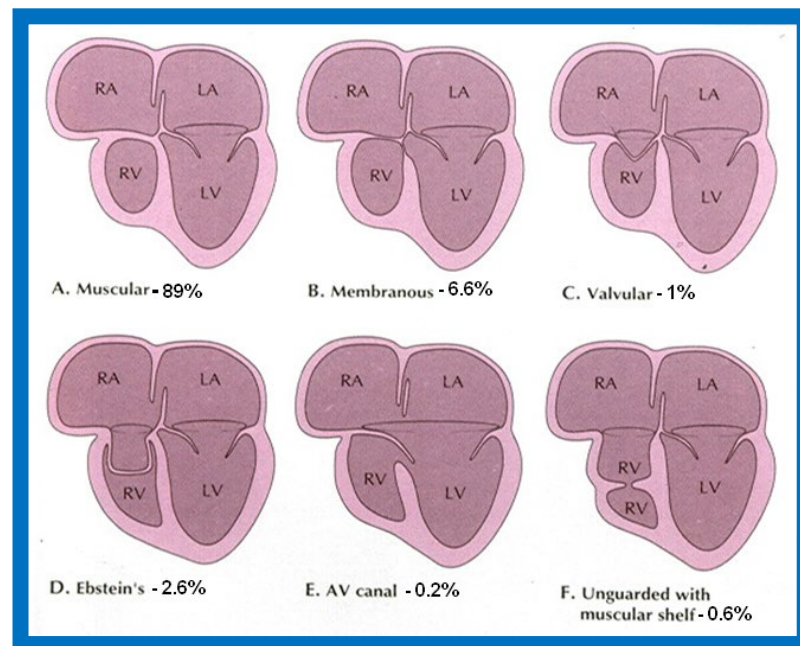


Figure 1. Diagrammatic portrayal of anatomic types of tricuspid atresia based on the morphology of the atretic tricuspid valve. (A) muscular type, (B) membranous type, (C) valvular type, (D) Ebstein's type, (E) atrioventricular canal type, and (F) unguarded valve with muscular shelf. The prevalence of each type is shown under each diagram. For the sake of simplicity, the great vessels are not shown. Also note that no ventricular septal defects are shown. LA, left atrium; LV, left ventricle; RA, right atrium; RV right ventricle. Modified from Rao PS, Alapati S. *Neonatology Today* 2012;7(5):1–12 [11].

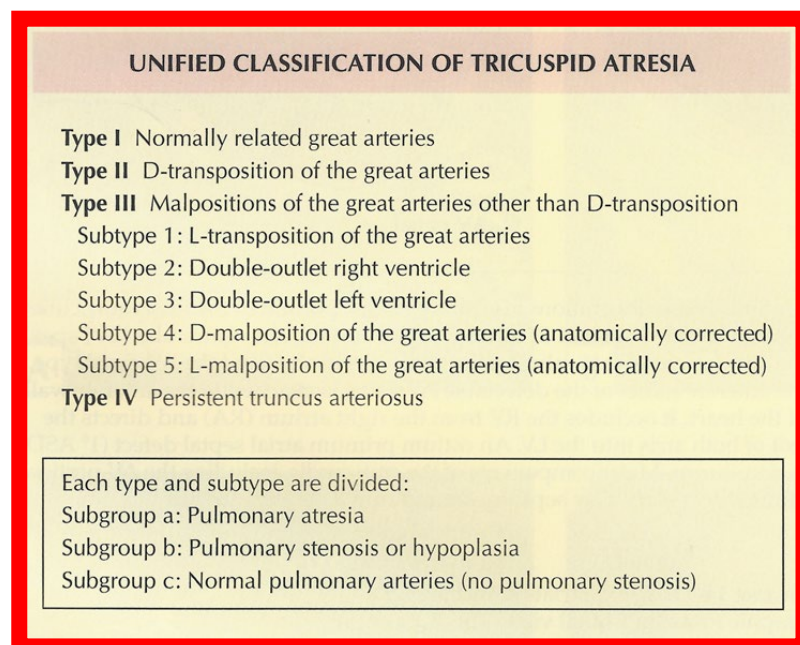


Figure 2. Classification of Tricuspid Atresia. Reproduced from [12].

The right atrium (RA) is enlarged and the atretic tricuspid valve is seen as a dimple or a localized fibrous thickening in the floor of the right atrium at the anticipated site of the tricuspid valve [10]. An inter-atrial defect is necessary for survival and is typically a stretched patent foramen ovale (PFO). However, occasionally, an ostium secundum atrial septal defect (ASD) or an ostium primum ASD may be present, facilitating right to left shunt. The left atrium (LA) is enlarged, especially when the pulmonary blood flow is increased. The mitral

valve is usually bicuspid and, morphologically, a mitral valve. However, its orifice is large and occasionally incompetent. The left ventricle (LV) is evidently a morphological LV, but it is enlarged and hypertrophied. The right ventricle (RV) is hypoplastic and is not sufficiently large in size to support pulmonary circulation in most patients.

The ventricular septum is intact in a rare patient, but, usually, a ventricular septal defect (VSD) is present; this may be large or small, or multiple VSDs may be seen. The VSD may be: conoventricular or perimembranous, located inferior to the septal band; a conal septal malalignment type, located in between the anterosuperior and posteroinferior limbs of the septal band; muscular, located inferiorly in the muscular septum; or, rarely, of an atrioventricular canal type. In the author's personal experience, VSDs are most commonly seen in the muscular septum, are restrictive [14–16] and cause subpulmonary obstruction in Type I patients and potential subaortic stenosis in Type II patients [14–21].

The great vessel relationship is variable, as discussed above (Figure 2, top). The ascending aorta is either normal or slightly larger than normal. The RV outflow tract is atretic, narrowed, or normal, depending upon the subgroup (a, b, or c). In patients with normally related great arteries (Figure 2), the obstruction to pulmonary blood flow is frequently at the VSD level although subvalvar or valvar (very rare) pulmonary stenosis or the narrow tract of the hypoplastic RV may occasionally be responsible for such obstruction. In cases with the transposition of the great arteries (Type II), the pulmonary obstruction is usually subvalvar. In cases with pulmonary atresia, either a patent ductus arteriosus (PDA) or aortopulmonary collateral vessels are present. Other abnormalities may be present in nearly 30% of tricuspid atresia cases [22]; significant of these are the coarctation of the aorta (in Type II - transposition cases) and persistent left superior vena cava, which have therapeutic implications.

3. Historical Aspects of the Evolution of the Echo of TA

At the time of the preparation of the manuscript for the author's first edition of the book on tricuspid atresia [23], two dimension (2D) echocardiography was being introduced into clinical practice and the 2D pictures were crude, requiring us to juxtapose line drawings [24] to facilitate interpretation of the figures (Figure 3). The published 2D pictures of TA [25,26], prior to ours, were equally crude. These pictures [24–26] represented the state of the art echocardiography machines of that time.

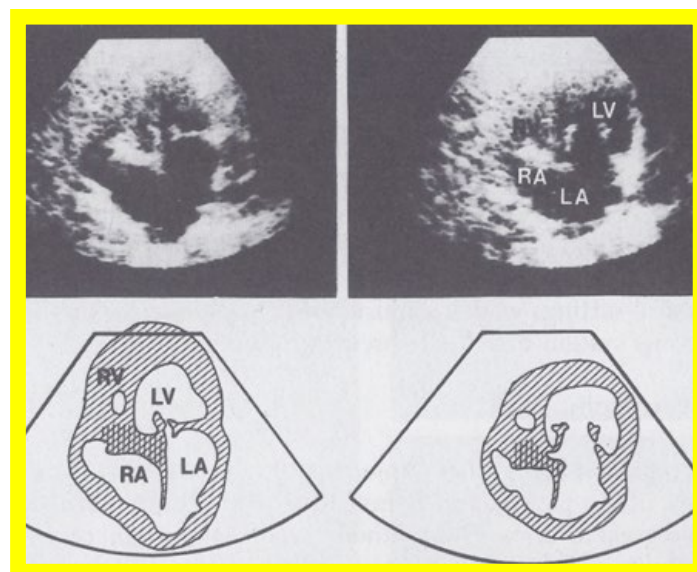


Figure 3. Selected video frames from apical four chamber view of a two dimensional (2D) echocardiographic study, demonstrating a dense band of echoes between the right atrium (RA) and hypoplastic right ventricle (RV). Line drawings are shown beneath the 2D frames. Note that the mitral valve is closed in the left image, while it is open in the right image. The atretic tricuspid valve echoes remain unchanged. LA, left atrium; LV, left ventricle. Reproduced from Reference [24].

Subsequently, improved echocardiography equipment resulted in producing progressively better images [27–29] (Figures 4–6).

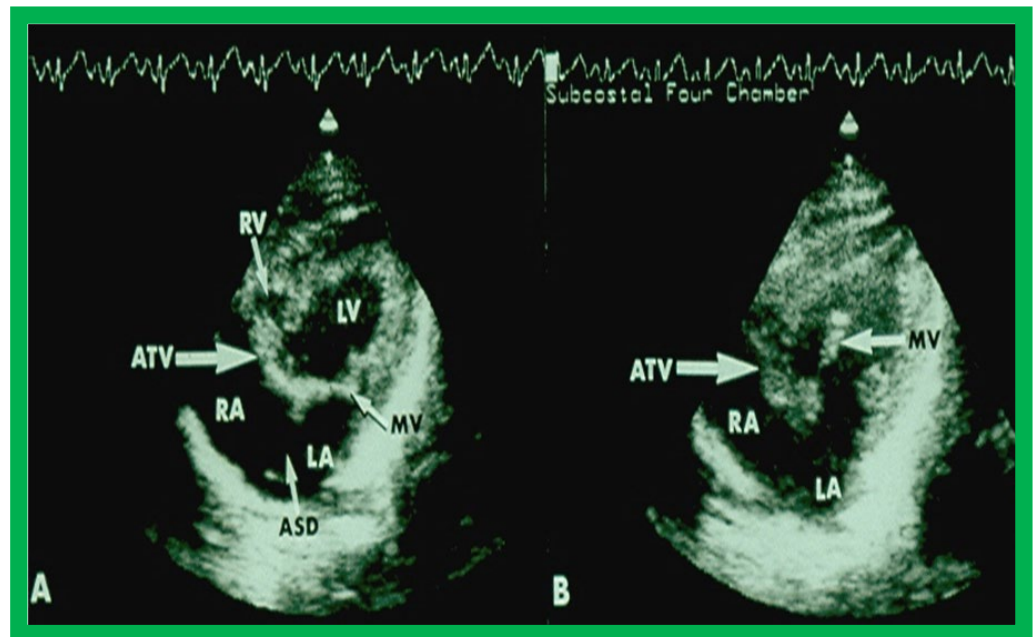


Figure 4. Selected video frames from subcostal four chamber view of a two dimensional echocardiographic study demonstrating an atretic tricuspid valve (ATV) (thick arrow), represented by a dense band of echoes between the right atrium (RA) and hypoplastic right ventricle (RV). In (A), the mitral valve (MV) is closed while in (B), it is open. Note the improvement from the pictures shown in Figure 2. LA, left atrium; LV, left ventricle. Reproduced from Reference [27].

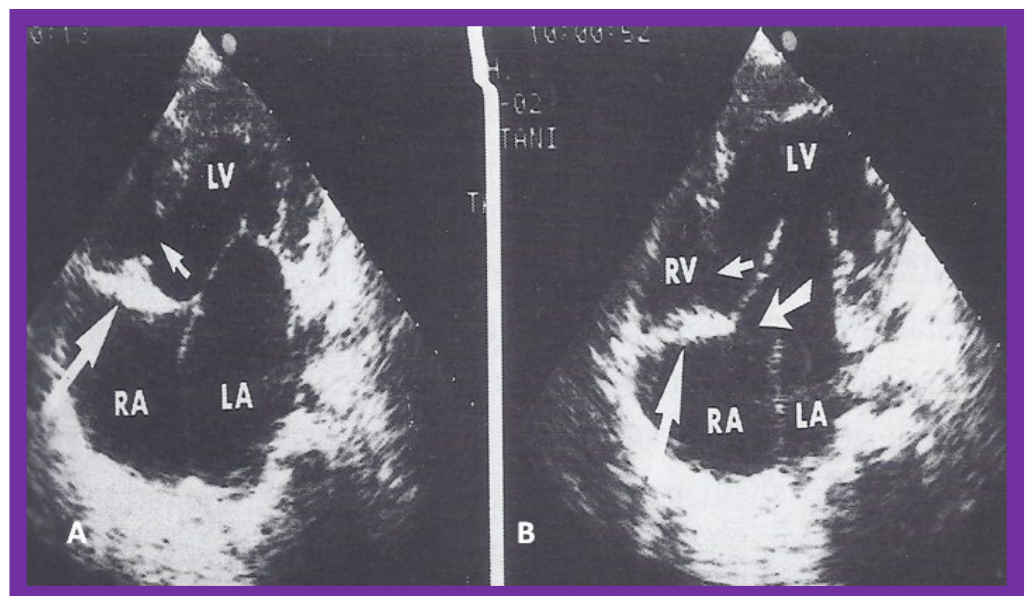


Figure 5. Apical four chamber view pictures of an infant with tricuspid atresia with ostium primum atrial septal defect (large arrow in the middle of (B)). Note the small right ventricle (RV) and a ventricular septal defect (small arrow in (A,B)). LA, left atrium; LV, left ventricle; RA, right atrium. Reproduced from Reference [28].

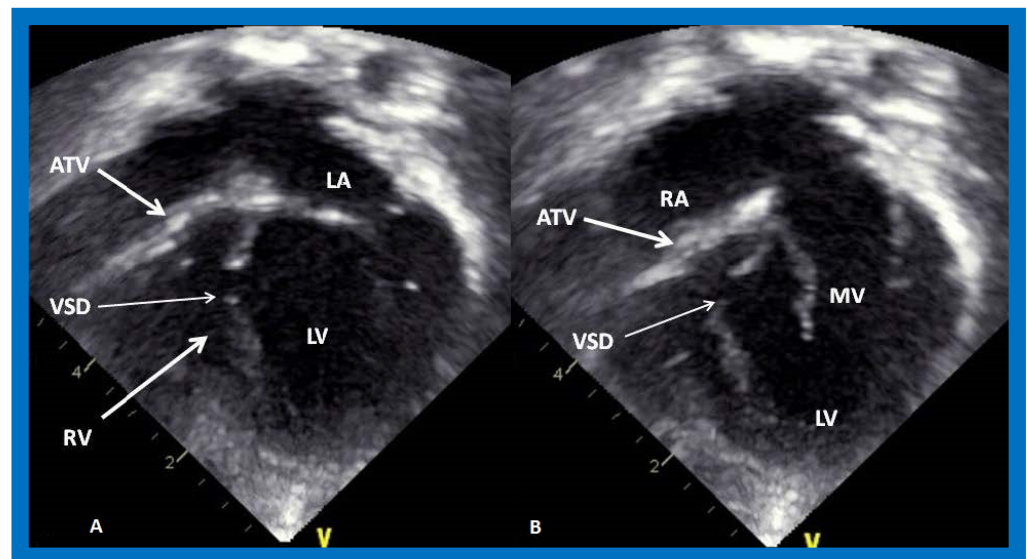


Figure 6. Selected video frames from apical four chamber, two dimensional echocardiographic views of a patient with tricuspid atresia showing an enlarged left ventricle (LV), a small right ventricle (RV) and a dense band of echoes at the site where the tricuspid valve echo should be (ATV) (thick arrow) with a closed (A) and open (B) mitral valve. A moderate sized ventricular septal defect (VSD) (thin arrow) is shown. LA, left atrium; RA, right atrium. Reproduced from Reference [29].

4. Echo-Doppler Features of TA on the Basis of Current Technology

On 2D echocardiography, the atretic tricuspid valve is visualized directly as a dense band of echoes at the site where the tricuspid valve should be, as shown in Figures 4–6; this echo appearance is that of the most frequent muscular type of TA. This anatomy is better demonstrated in apical and subcostal four chamber views than in other views. The other anatomic types (Figure 1), namely, membranous, valvular, Ebstein's, atrioventricular septal defect, and unguarded tricuspid valve with muscular shelf, are rare and may also be recognized on 2D echocardiography. An example of an atrioventricular septal defect type of TA [30] is demonstrated in Figure 7; in this example, a 2D echocardiogram demonstrated an ostium primum ASD with a common atrioventricular valve and a small RV (Figure 7a,b); the entry into the RV appeared to be occluded by a leaflet of the common atrioventricular valve. Left ventricular and right atrial cineangiograms confirmed these findings [30]. Evaluation of the crux cordis (Figure 8) on a 2D echocardiogram (subcostal four chamber view) may help to distinguish the various anatomic types (Figure 1) from each other. In the muscular type of tricuspid atresia, a dense band of echoes is seen where the normal tricuspid valve should be (Figure 8A). In membranous types of tricuspid atresia, a thin membrane is seen instead (Figure 8B). In both these types, the anterior leaflet of the detectable atrioventricular valve is attached to the left side of the interatrial septum (Figure 8A,B). In the atrioventricular septal defect type of tricuspid atresia, the crux cordis is abnormal and cannot be identified; the anterior leaflet of the detectable atrioventricular defect is attached to the anterior wall of the heart, and a large atrioventricular valve leaflet occludes the entry of the RA into the RV (Figure 8C). Based on these observations, it was concluded that 2D echocardiographic (and angiographic) features help to differentiate the atrioventricular canal type of tricuspid atresia from the classic muscular tricuspid atresia cases [30].

Following the demonstration of the atretic tricuspid valve, the sizes of the cardiac chambers are evaluated both by M-mode (Z scores) and 2D echocardiography; an enlarged RA, LA and LV and a small RV are seen (Figures 4–6). Pulsed (not shown) and color Doppler (Figure 9) studies are helpful in illustrating right to left shunt across a PFO or an ASD.

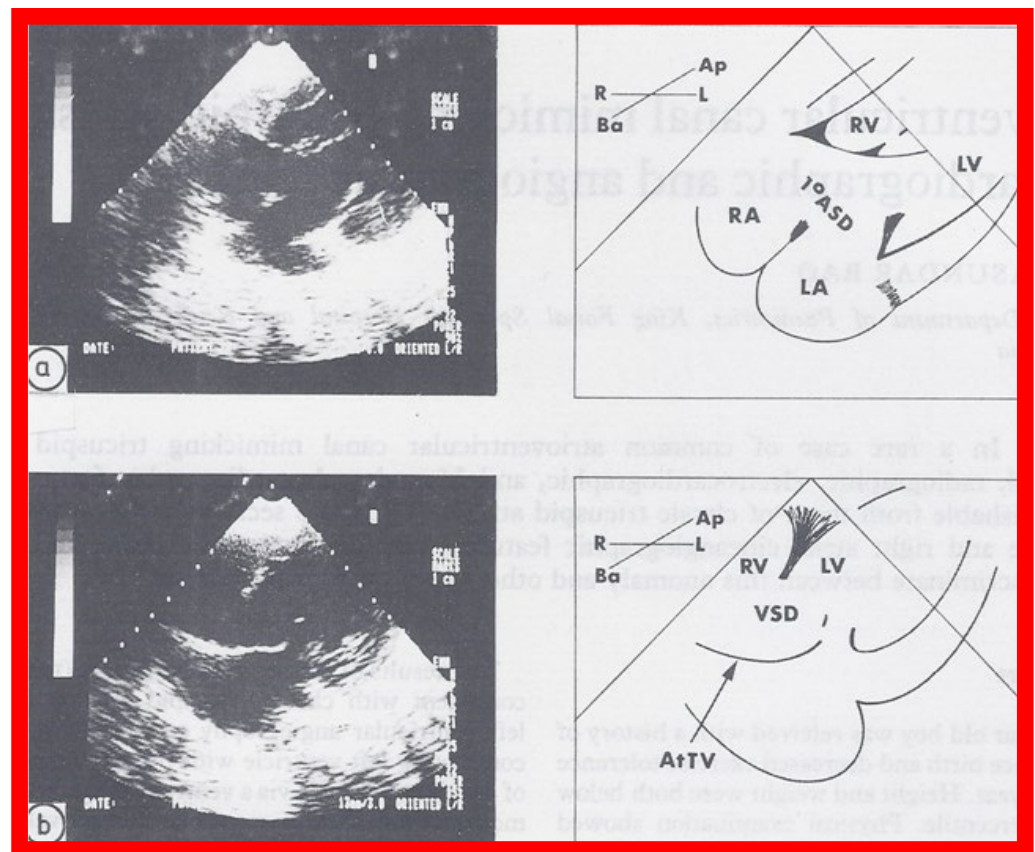


Figure 7. Selected two dimensional, subcostal, four chamber echocardiographic frames with an open (a) and closed (b) atrioventricular valve. Line drawings on the right of (a,b) are made for greater clarity and for labeling. A large ostium primum atrial septal defect (1° ASD) is shown in (a). When the large atrioventricular valve leaflet is open (a), it completely closes the right ventricle (RV) from the right atrium (RA) and the ventricular septal defect (VSD) and allows the emptying of blood from both atria into the left ventricle (LV). When the atrioventricular valve leaflet is closed, (b), it continues to occlude the RV from the RA while allowing the VSD to freely communicate between the RV and LV. Ap, Apex; AtTV, atretic tricuspid valve; Ba, base; L, left; LA, left atrium; R, right. Reproduced from Rao PS. *Brit Heart J* 1987;58:409–412 [30].

The relationship of the great arteries is examined next in order to classify them into various types, as mentioned above. The relationship of the great arteries (Figure 2, top) is established by following the vessels arising from the ventricles until the pulmonary artery (PA) bifurcation or aortic arch. In Type I patients with normally related great arteries, the aorta arises from the LV (Figure 10) and in Type II patients with transposition of the great arteries, the PA arises from the LV (Figure 11; Figure 12). In Type II patients, the blood vessel arising from the LV should be traced to demonstrate its branching into the right and left PAs (Figure 11; Figure 12). In Type III patients, it may be a little more difficult to assign the great artery relationship and, sometimes, other imaging studies, including angiography, may be needed to define the great artery relationship. In Type IV with truncus arteriosus, the limited data suggest that this can be performed by echocardiography (Figure 13; Figure 15). In the example shown [31], the atretic tricuspid valve (Figures 13a and 14a), VSD (Figures 13b and 14b), hypoplastic RV (Figure 14a), single vessel (truncus) arising from the heart (Figures 13c,d, and 14c,d), and origin of the PA and its division into branch PAs (Figures 13d, and 14c,d) were demonstrated.

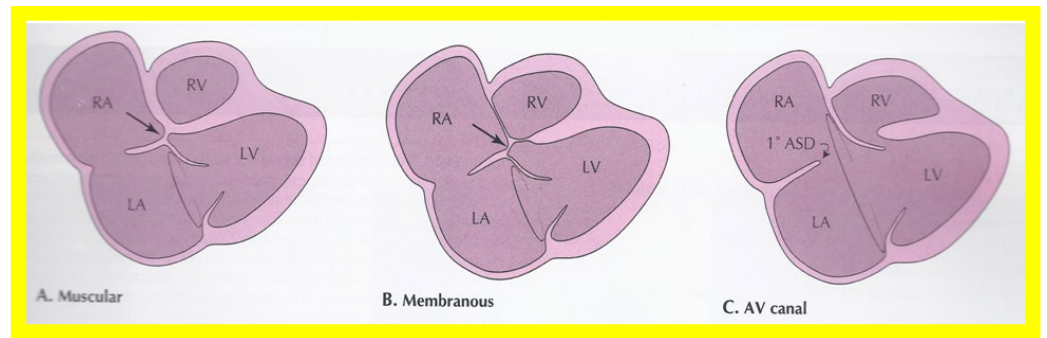


Figure 8. Line drawings demonstrating two dimensional echocardiographic appearances in a subcostal four chamber view of the muscular (A), membranous (B), and atrioventricular canal (C) variants of tricuspid atresia. (A) The atretic tricuspid valve is represented by a thick band of echoes between the right atrium (RA) and the small right ventricle (RV) in the muscular type. (B) The tricuspid valve is represented by a thin line in the membranous type. Note that crux of the heart (arrows in (A,B)) is clearly seen in both these types (A,B). The attachment of the anterior leaflet of the detectable atrioventricular valve to the left side of the interatrial septum is evident. (C) In the atrioventricular canal type of tricuspid atresia, the anterior leaflet of the detectable atrioventricular canal is attached to the anterior wall of the heart, occluding the right ventricle from the right atrium, and allows the exit of blood from both atria into the left ventricle (LV). The crux cordis and the atrioventricular portion of the interventricular septum are not seen. Reproduced from Rao PS. *Brit Heart J* 1987;58:409–412 [30] and from Reference [12].

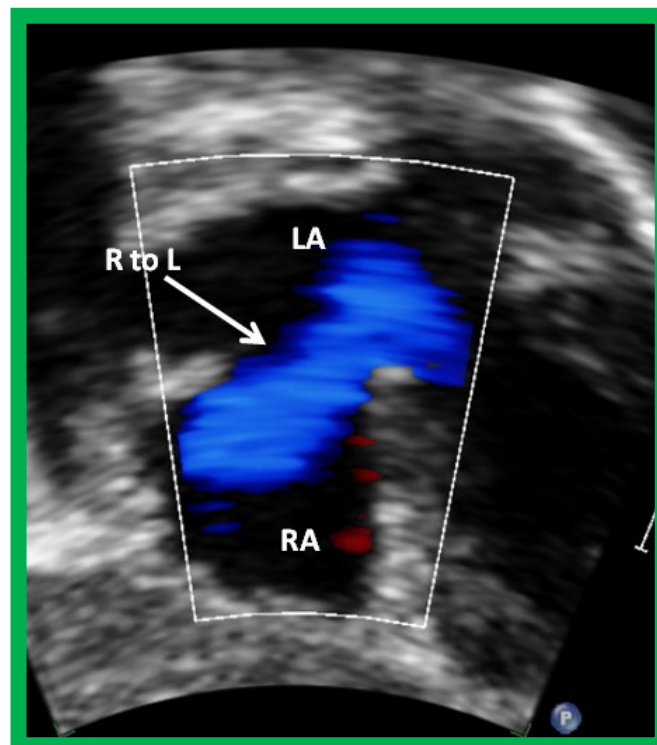


Figure 9. Selected video frame from subcostal view of a patient with tricuspid atresia demonstrating right to left (R to L) shunt (arrow) across the interatrial communication. LA, left atrium; RA, right atrium. Reproduced from Reference [29].

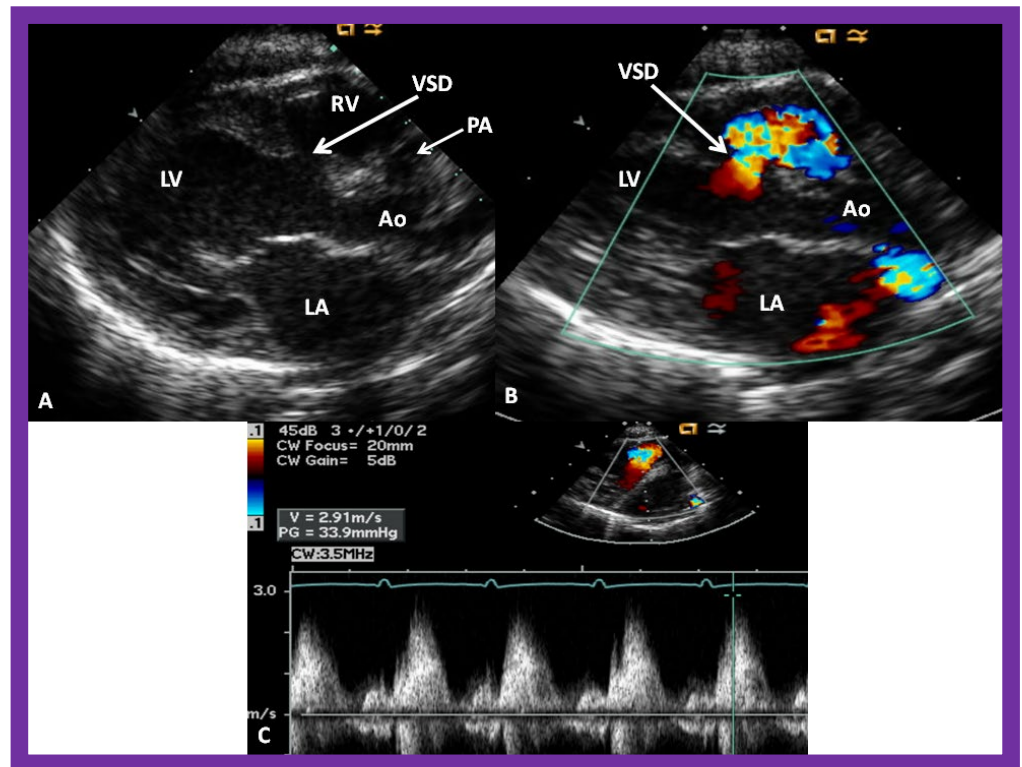


Figure 10. Selected video frames from parasternal long axis views of a patient with tricuspid atresia with normally related great arteries demonstrating an enlarged left atrium (LA) and left ventricle (LV), a small right ventricle (RV) and a moderate sized defect (VSD) (thick arrow) on 2D (A) and color flow (B) imaging. The turbulent flow (B), with a Doppler flow velocity of 2.91 m/s by continuous wave Doppler (C) across the VSD, suggests some restriction of the VSD. Ao, Aorta; PA, pulmonary artery. Reproduced from Reference [29].

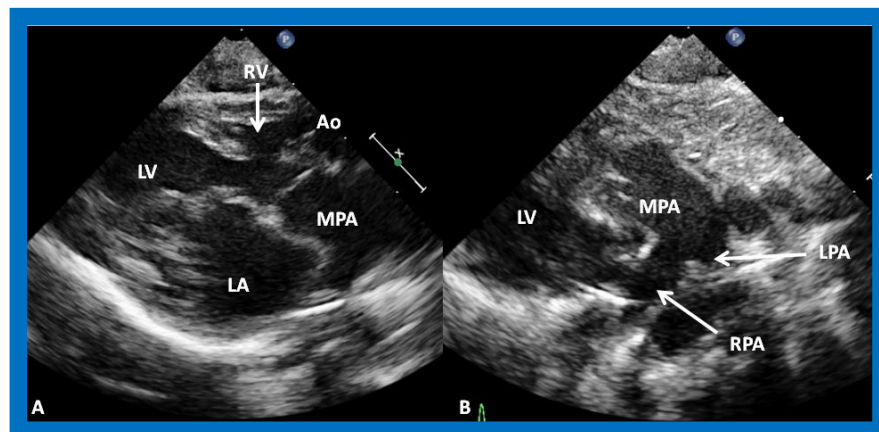


Figure 11. (A) A selected video frame from parasternal long axis views of a patient with tricuspid atresia and transposition of the great arteries demonstrating the left atrium (LA), left ventricle (LV), a very small right ventricle (RV) and a moderate sized ventricular septal defect (not marked). The vessel coming off the LV is traced in (B) and shown to bifurcate into the left (LPA) and right (RPA) pulmonary arteries, confirming that this vessel is the main pulmonary artery (MPA), consistent with transposition of the great arteries. Ao, Aorta. Reproduced from Reference [29].

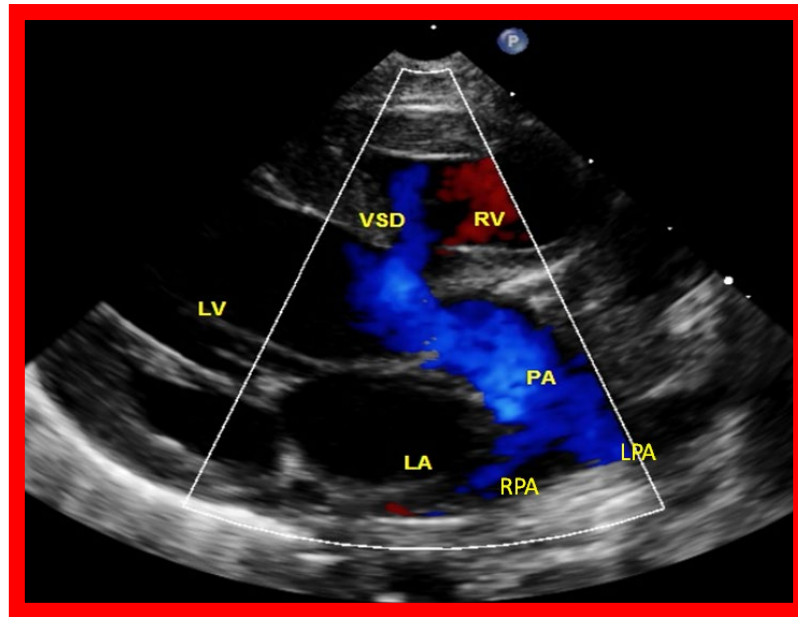


Figure 12. A selected video frame from a parasternal long axis view with color flow mapping of another patient with tricuspid atresia and transposition of the great arteries demonstrating the left atrium (LA), left ventricle (LV), a small right ventricle (RV) and a moderate sized ventricular septal defect (VSD). The vessel coming off the LV bifurcates into right (RPA) and left (LPA) pulmonary arteries. Reproduced from Reference [29]. PA, pulmonary artery.

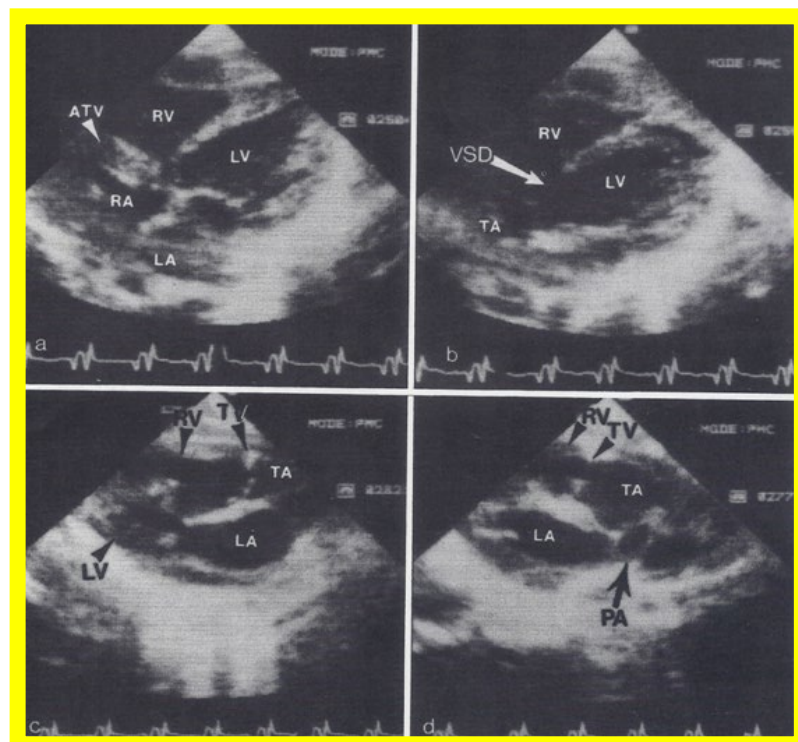


Figure 13. Two dimensional echocardiographic video frames demonstrating (a) an atretic tricuspid valve (ATV) between the right atrium (RA) and right ventricle (RV), (b) a large subtruncal ventricular septal defect (VSD), (c) thickened and somewhat domed truncal valve (TV) leaflets, and (d) the origin of the pulmonary artery (PA) from the posterior aspect of the truncus arteriosus (TA). LA, left atrium; LV, left ventricle. Reproduced from Rao PS, et al. *Am Heart J* 1991;122:829–835 [31].

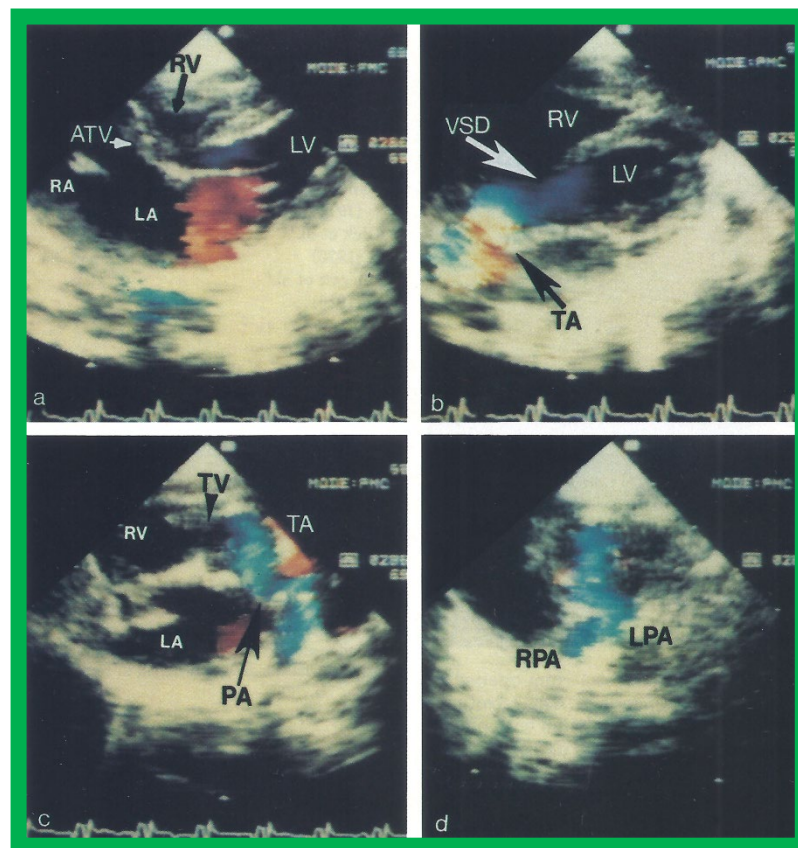


Figure 14. Video frames from a two dimensional echocardiographic and color Doppler study demonstrating (a) an atretic tricuspid valve (ATV) between the right atrium (RA) and right ventricle (RV), and blood flow from the left atrium (LA) into the left ventricle (LV) across the mitral valve. The RV (arrow) is very small and hypoplastic. (b) LV and RV with a large ventricular septal defect (VSD) below the truncus arteriosus (TA). Turbulent flow across the truncal valve suggests truncal valve stenosis. (c) The origin of the pulmonary artery (PA) from the TA by color flow (arrow), and (d) the division into right (RPA) and left (LPA) pulmonary arteries from the PA in a short-axis view. TV, truncal valve leaflets. Reproduced from Rao PS, et al. *Am Heart J* 1991;122:829–835 [31].

Further subdivision (Figure 2, bottom) into subtypes a (pulmonary atresia), b (pulmonary stenosis or hypoplasia), and c (normal valve and pulmonary arteries) is undertaken by echo-Doppler examination of the pulmonary valve and PAs, irrespective of the types, I, II, III or IV.

Then, the ventricular septum is evaluated; the ventricular septum is intact in most Type Ia cases. In children with Type I (normally related great arteries), the VSD supplies the pulmonary blood flow (Figure 10) while in patients with Type II (transposition of the great arteries) the VSD allows the blood to flow into the systemic circuit (Figure 11; Figure 12). In Type I patients, the VSD is demonstrated by 2D (Figure 10A), and the left to right shunt across it by color (Figure 10B), pulsed and CW (Figure 10C) Doppler signals. The interrogation of the RV outflow tract and PA region should be performed; recording the peak Doppler flow velocity across the RV outflow tract and the pulmonary valve is helpful in identifying obstruction across these sites. The Doppler data from the VSD and RV outflow tract are also helpful in the estimating of PA pressures. In Type I babies, the 2D size of the VSD and the peak Doppler flow velocity across it are useful in quantifying the size of the VSD (Figure 10). The higher the VSD Doppler flow velocity, the smaller the defect. However, in patients with pulmonary hypertension or severe infundibular or valvar pulmonary stenosis, the VSD Doppler velocities are not reflective of the size of the VSD. Barring these exceptions, RV and PA systolic pressure may be estimated using a modified Bernoulli equation ($RV/PA \text{ systolic pressure} = \text{systolic blood pressure} - 4V^2$).

In Type II patients, the VSD may be small, causing obstruction to blood flow to the systemic circuit, and, therefore, the size of the VSD should be ascertained by 2D (Figures 11 and 12), color Doppler (Figure 12), pulsed (Figure 15) and CW Doppler, as necessary. In these Type II patients, a high VSD velocity is indicative of subaortic obstruction. Interrogation of the LV outflow and PA region may reveal pulmonary or subpulmonary stenosis; the higher the velocity, the more severe is the obstruction. Studies from the suprasternal notch may show aortic coarctation (Figure 16), which is common in patients with Type II anatomy.

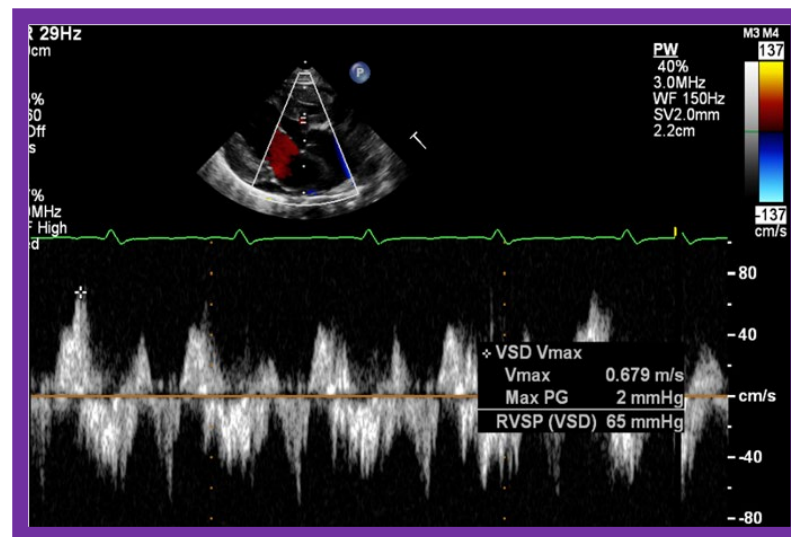


Figure 15. Selected video frame of continuous wave Doppler across the ventricular septal defect of the same patient, as is shown in Figure 11. The low velocity flow across the ventricular septal defect suggests that the defect is nonobstructive. Reproduced from Reference [29].

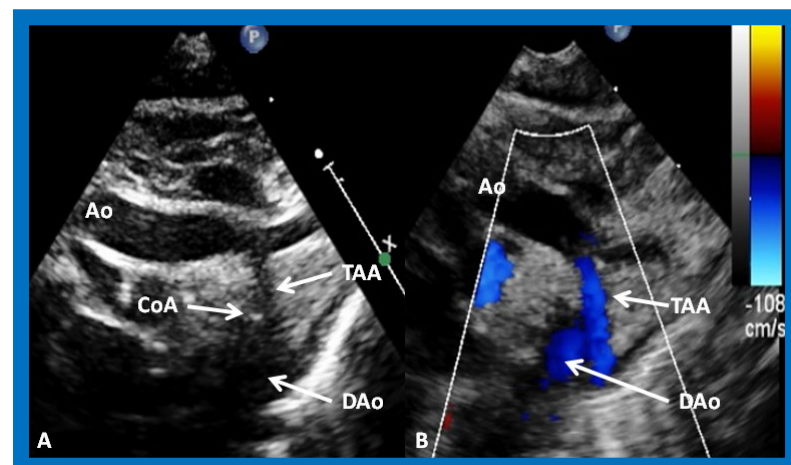


Figure 16. Selected video frames from suprasternal notch views of the aortic (Ao) arch in 2D (A) and color flow (B) images of a neonate with tricuspid atresia and transposition of the great arteries, demonstrating coarctation of the aorta (CoA) and a hypoplastic transverse aortic arch (TAA) and isthmus. The association of CoA with tricuspid atresia, plus transposition of the great arteries, is well known. DAo, descending aorta. Reproduced from Reference [29].

A large number of other cardiac defects are known to be associated with tricuspid atresia (Table III—Reference [22]). Consequently, echo-Doppler studies should be scrutinized for these defects during echo evaluation.

Contrast study following the venous injection of agitated saline during 2D imaging clearly demonstrates the successive opacification of the RA, LA, LV and then the RV, in that order, but such a study is not necessary for diagnosis and is not routinely performed.

In summary, the delineation of the majority of anatomic and physiologic issues related to TA is feasible by M-mode, 2D, and Doppler (pulsed, continuous wave, and color) echocardiography, and, consequently, magnetic resonance imaging (MRI), computed tomography (CT), and cardiac catheterization with selective cineangiography are not necessary for the confirming of the diagnosis. In addition, the echo-Doppler studies can help define pathophysiologic features relevant in the management of TA patients.

5. Echo-Doppler Studies Following Palliative/Corrective Interventions

Prior to reviewing the echo-Doppler findings seen following palliative/corrective interventions, the presentation of a summary of palliative and corrective transcatheter/surgical procedures for TA is in order.

5.1. Summary of Palliative/Corrective Interventions

Total surgical correction is not feasible for patients with TA. However, physiologic correction is feasible, which was described in the early 1970s by Fontan [32] and Kreutzer [33] and their associates, concurrently. Since its early description in the 1970s, the Fontan procedure has undergone a number of modifications, as reviewed elsewhere [34–38]. Currently, total cavopulmonary connection, advocated by de Leval and his colleagues [39], is routinely performed. Due to high PA pressure/resistance in the neonates, the procedure cannot be performed in neonates and young infants. Therefore, it is undertaken in three stages: Stage I. Palliation at the time of initial presentation, usually in the neonatal period (see below); Stage II. Bidirectional Glenn [40] between 3 and 12 months of age (along with the ligation of prior aorto-pulmonary shunt); and Stage III. Fontan completion one to two years later by redirecting the IVC blood flow into the PAs, either via a lateral tunnel [41] or via an extracardiac nonvalved conduit [41,42]. Most of the Fontan procedures performed today include a fenestration [43,44]. The fenestration may be closed at a later date by a transcatheter methodology [36–38,43]. Staged, total cavopulmonary connection with an extracardiac nonvalved conduit and fenestration has become standard of care for all single ventricle lesions, including TA [36–38].

Most of the patients with TA require symptomatic relief at initial presentation [22]. Babies with pulmonary oligemia are addressed with initial Prostaglandin E₁ infusion, followed by a modified Blalock-Taussig shunt operation [45] or other types of aorto-pulmonary Gore-Tex graft shunts. Infants with pulmonary plethora are treated with anticongestive measures (if they are in congestive heart failure (CHF)) followed by the banding of the PA [46]. In some Type II (transposition of the great arteries) patients, the VSD may be small and obstructive, and is usually treated with Damus-Kaye-Stansel (DKS) procedure. Some patients may develop inter-atrial obstruction requiring balloon atrial septostomy [47–49], and others may need the relief of aortic coarctation. A few patients may have adequate pulmonary blood flow and need no intervention in the neonatal period.

5.2. Echocardiographic Evaluation Following Neonatal Palliative Procedures

Following palliation, the LV size and function should be monitored, adequacy of the atrial defect to maintain unrestricted right to left shunt should be scrutinized (to ensure no development of restriction), and effectiveness of palliative procedures should be evaluated.

5.2.1. LV Size and Function

In most patients, LV size and function (Figure 17) remain within normal range, although large surgical shunts and inadequate PA banding may result in the deterioration of LV function. Consequently, periodic echo studies to monitor LV systolic function are recommended.

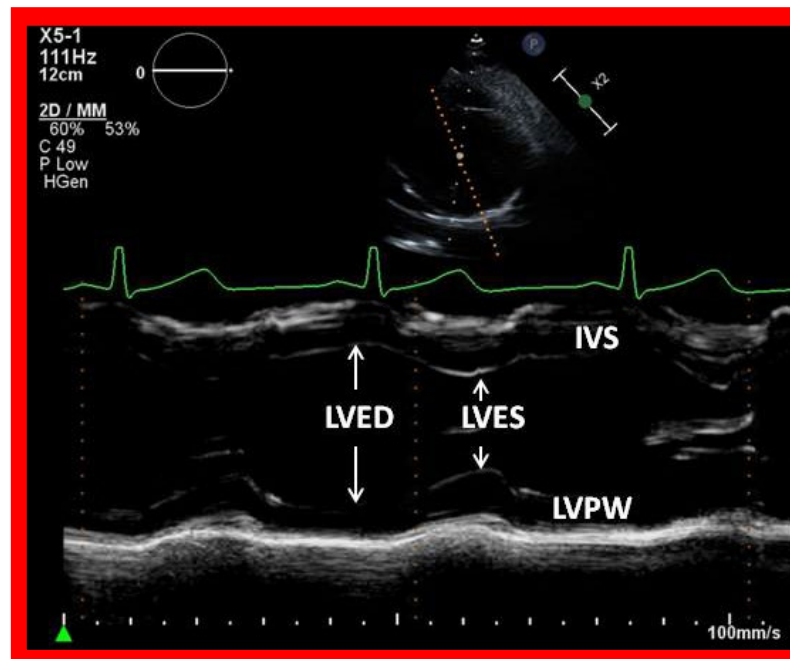


Figure 17. Selected video frame showing left ventricle in end diastole (LVED) and in end systole (LVES) demonstrating normal function. IVS, interventricular septum; LVPW, left ventricular posterior wall.

5.2.2. Adequacy of the ASD/PFO

Echo-Doppler studies should examine the adequacy of PFO/ASD to decompress the RA and allow unrestricted flow across it. In the majority of TA patients, the PFO/ASD remains wide open with unrestricted right to left shunt across it with laminar flow (Figure 18). This appears to be secondary to the persistence of fetal circulatory pathways. Only rarely does significant obstruction requiring intervention develop.

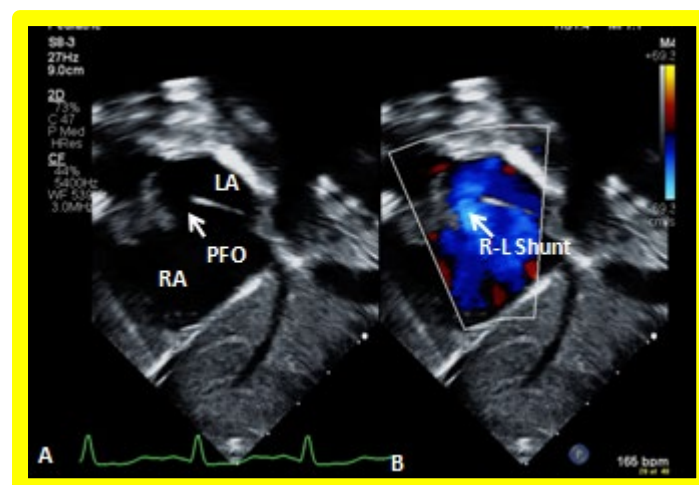


Figure 18. Selected video frames from a subcostal echocardiographic study demonstrating patent foramen ovale (PFO) (arrow in (A)) with right to left shunt (R-L Shunt) across the PFO (arrow in (B)). Note laminar flow across the PFO in B. LA, left atrium, RA, right atrium.

5.2.3. Effectiveness of Palliative Procedures

In patients who had an aorto-pulmonary shunt (most commonly modified Blalock-Taussig), the shunt may be visualized by color flow imaging (Figure 19), although it is difficult to image it only by 2D. High Doppler flow velocities across the shunt are normally recorded (Figure 20), and they reflect the systolic pressure difference between the aorta

and PAs. Low Doppler flow velocities across the shunt, however, may indicate high PA pressures. The flow into branch PAs can easily be demonstrated by color flow Doppler imaging (Figure 19B). Flow acceleration in the branch PAs is usually seen (Figure 21) and is of no concern. However, high flow velocities may indicate branch PA stenosis.

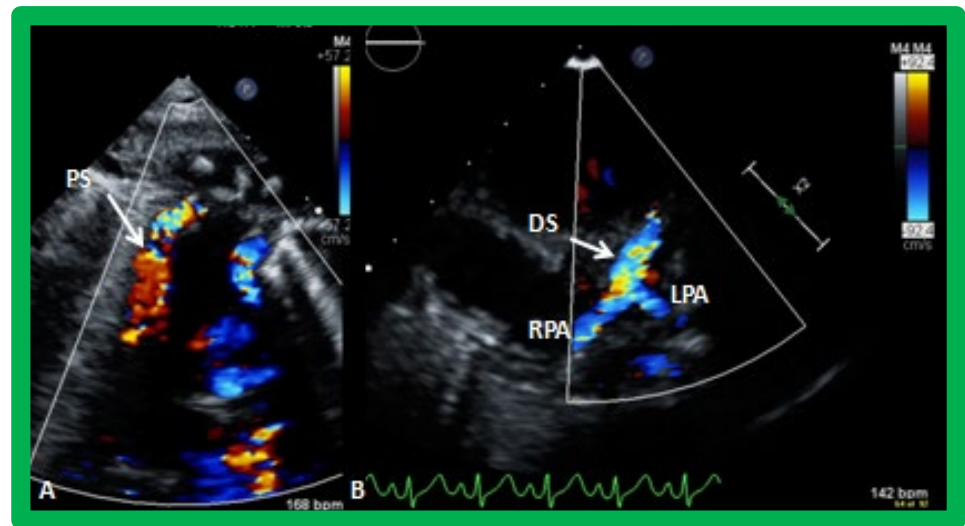


Figure 19. Selected video frames from suprasternal notch view demonstrating proximal shunt (PS) by color flow imaging (A). In a slightly different view, (B), the flow from the distal shunt (DS) into right (RPA) and left (LPA) pulmonary arteries is shown.

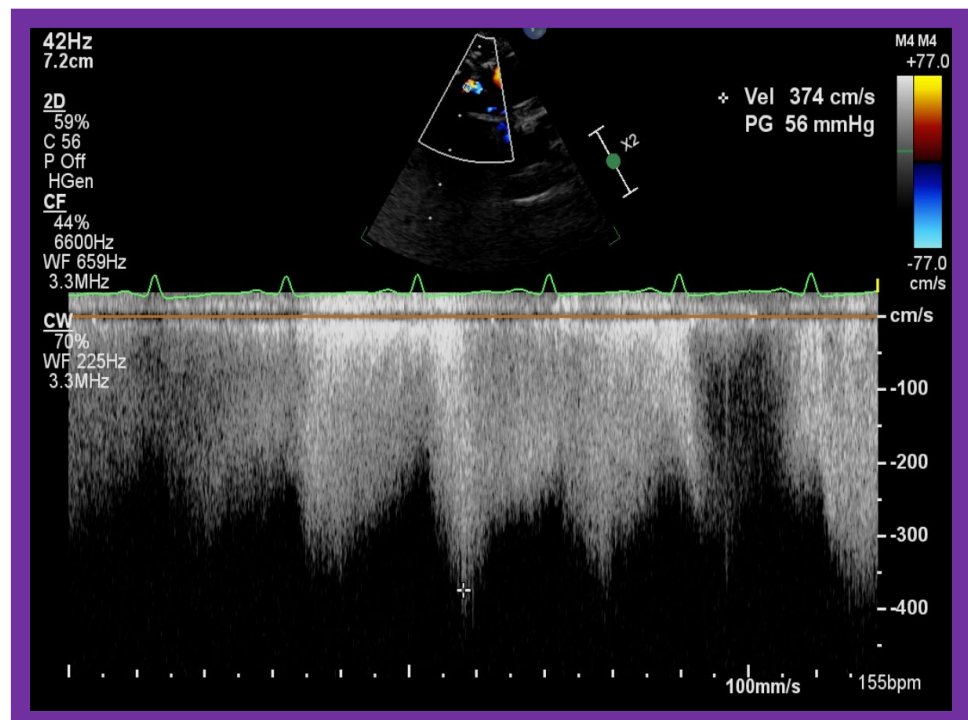


Figure 20. Selected video frames from suprasternal notch view demonstrating high Doppler flow velocity across Blalock–Taussig shunt.

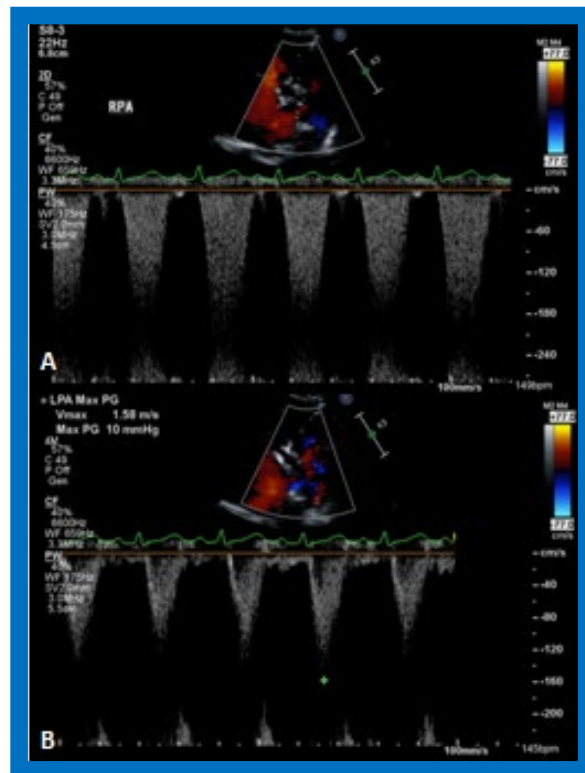


Figure 21. Selected video frames demonstrating flow acceleration across the right (RPA) (A) and left (LPA) (B) pulmonary arteries in a patient with a Blalock–Taussig shunt. These slightly higher than normal velocities do not indicate stenosis of the branch pulmonary arteries.

In patients who had banding of the PA, echo-Doppler studies should be scrutinized to demonstrate the banded PA diameter (Figure 22A,B and Figure 23A) and peak Doppler flow velocity across the banded PA (Figures 22C and 23B); high Doppler velocity across the band (Figures 22C and 23B) would suggest effective palliation. Low gradients and ineffective control of CHF may require tightening of the band; echo-Doppler evaluation is useful in making such an assessment.

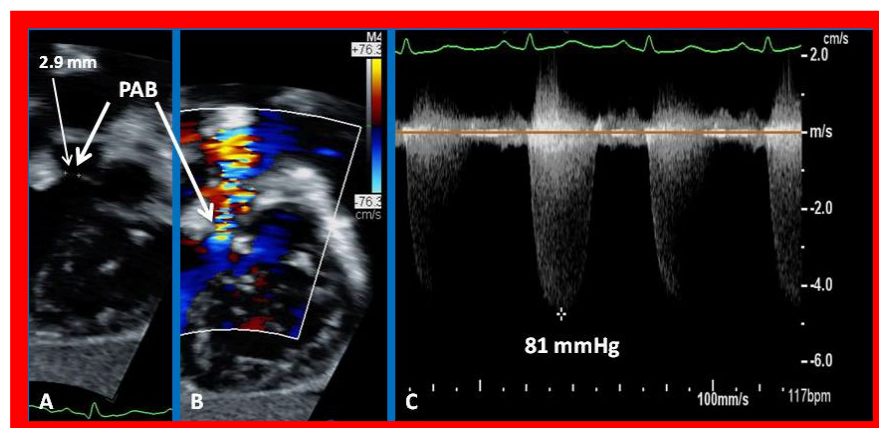


Figure 22. Selected echocardiographic video frames demonstrating pulmonary artery band (PAB) with narrow diameter of 2.9 mm by 2D (A) and by color flow (B) and a high gradient (81 mmHg) by continuous wave Doppler (C) are shown.

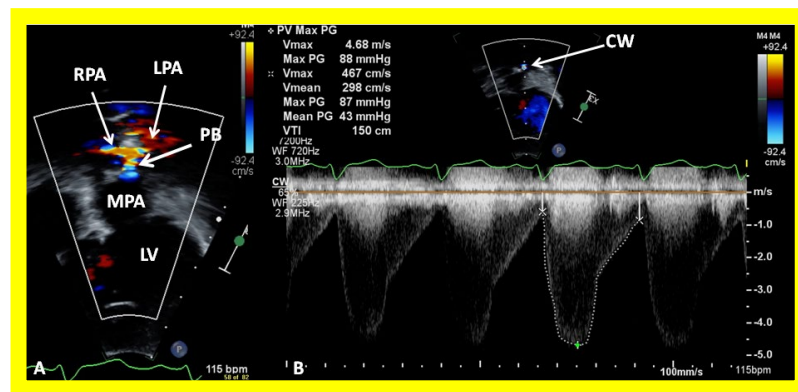


Figure 23. Selected echocardiographic video frames demonstrating pulmonary artery band (PAB) with narrow diameter by color flow (A) and a high gradient (88 mmHg) by continuous wave Doppler (B) are shown.

Angiographic counter parts of both the palliative procedures are shown in Figure 24, to have better comprehension of the anatomy of these procedures.

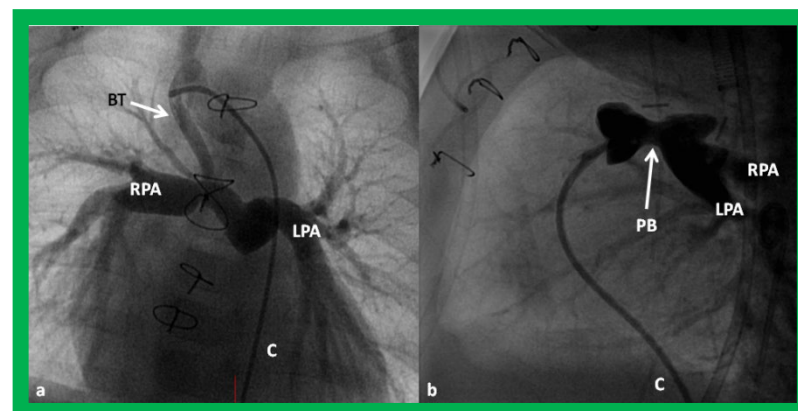


Figure 24. Selected cine frames in postero-anterior (a) and lateral (b) views, demonstrating a Blalock-Taussig (BT) shunt (arrow in a) to care for infants with decreased pulmonary blood flow (a) and pulmonary artery banding (PB) (arrow in (b)) in babies with increased pulmonary blood flow (b), respectively, during Stage I of Fontan procedure. C, catheter; LPA, left pulmonary artery; RPA, right pulmonary artery. Neonates with adequate pulmonary blood flow do not need any intervention and can go directly to Stage II at about the age of 3 months. Reproduced from Rao PS, *Indian J Pediatr* 2015;82:1147–1156 [36].

5.2.4. Echo Evaluation of Patients Who Did Not Have Any Intervention

Patients who have not had an intervention because of adequate pulmonary blood flow should also be monitored periodically with echo-Doppler studies until they have a bidirectional Glenn, to ensure that they maintain adequate pulmonary blood flow and that they do not develop other complications (see Section 5.4).

5.3. Echocardiographic Evaluation Following Bidirectional Glenn

Following bidirectional Glenn, the LV size is likely to decrease (normalize) and LV should maintain normal systolic function. This is because of decreased LV volume overload following bidirectional Glenn and the removal of aorto-pulmonary shunt. The 2D imaging of the bidirectional Glenn is difficult to accomplish, but color flow imaging (Figures 25A, 26B, and 27B) from a suprasternal notch or high parasternal views will help image the bidirectional Glenn. Low pulsed Doppler velocity across the superior vena cava (SVC)-PA junction (Figures 25B and 26C) would indicate no obstruction. Turbulent and high velocity Doppler flow suggests the obstruction of the bidirectional Glenn shunt.

The size of the branch PAs may be assessed with a combination of 2D and color flow imaging (Figures 26–28).

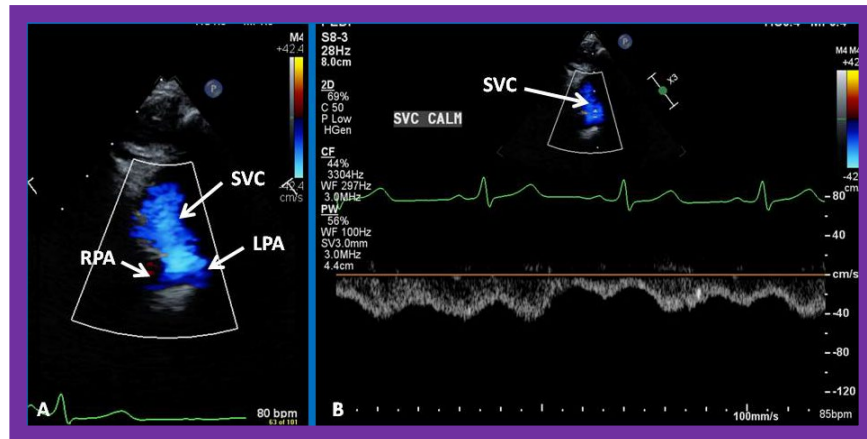


Figure 25. Selected video frames from suprasternal notch view demonstrating bidirectional Glenn shunt; the superior vena cava (SVC) is shown emptying into the right (RPA) and left (LPA) pulmonary arteries by color flow imaging (A). Low Doppler flow velocity across the shunt (B) indicates unobstructed Glenn.

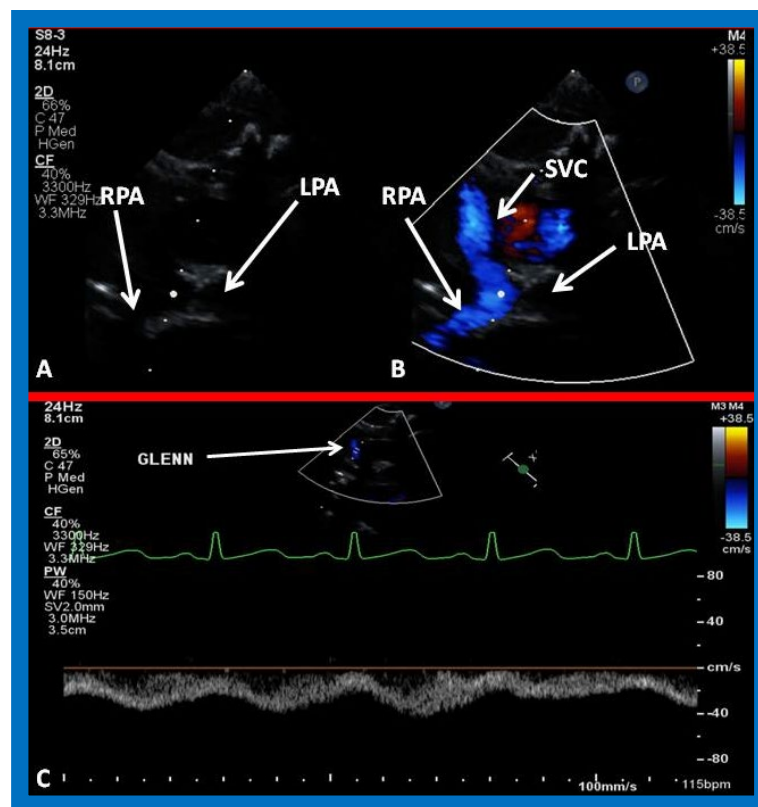


Figure 26. (A,B) Selected video frames from suprasternal notch view demonstrating bidirectional Glenn shunt. In (A), the right (RPA) and left (LPA) pulmonary arteries are shown by 2D. The superior vena cava (SVC) was not clearly seen. In (B), the SVC is shown emptying into the RPA by color Doppler (B). The LPA did not show color flow because it was in a different plane of imaging than RPA, but is seen by 2D (B). (C) Low Doppler flow velocity across the Glenn shunt indicates unobstructed flow.

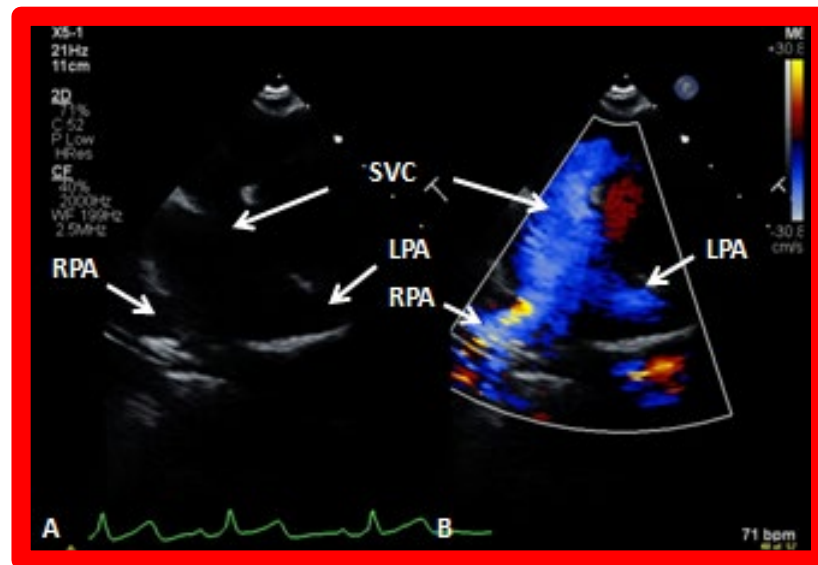


Figure 27. Selected video frames from suprasternal notch view demonstrating bidirectional Glenn shunt; the superior vena cava (SVC) is shown emptying into the right (RPA) and left (LPA) pulmonary arteries by two dimensional (A) and color flow imaging (B). Both RPA and LPA are seen with color in contrast to that seen in Figure 26, probably related to both pulmonary arteries are in a similar echo plane.

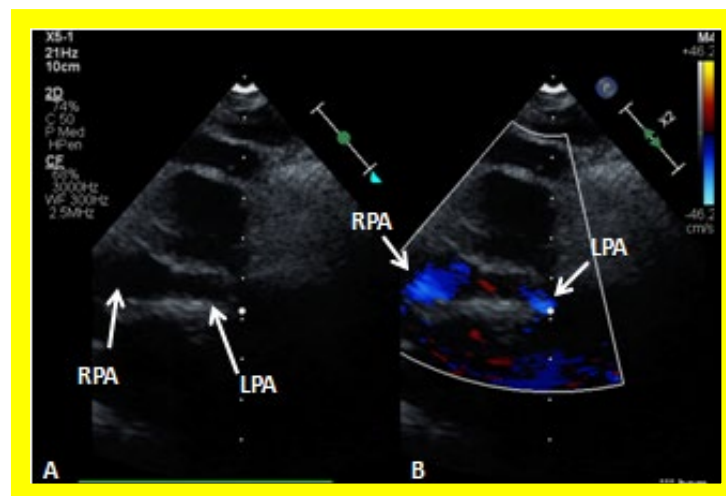


Figure 28. Selected video frames from suprasternal notch view demonstrating right (RPA) and left (LPA) pulmonary arteries without (A) and with (B) color flow imaging.

Angiographic counter parts of the bidirectional Glenn are shown, in Figure 29, to have better comprehension of the anatomy of the bidirectional Glenn.

In patients who have a persistent left SVC entering the heart via the coronary sinus, bilateral bidirectional Glenn procedures are performed, especially if the inter-connecting left innominate vein is small or absent. An example of left sided bidirectional Glenn is shown in Figure 30. In subjects who have infrahepatic interruption of the inferior vena cava (IVC) with azygos or hemiazygos continuation (into the right or left SVC, respectively), a Kawashima procedure is performed. In these patients, echocardiographic imaging of the Glenn/Kawashima is similar to that of regular bidirectional Glenn (Figures 25–27).



Figure 29. Selected cine frames in postero–anterior (a) and sitting up (b) views, demonstrating bidirectional Glenn procedure (the superior vena cava [SVC] is anastomosed with the right pulmonary artery [RPA]) in two different patients during Stage II of Fontan procedure. Unobstructed flow from the SVC to the right (RPA) and left (LPA) pulmonary arteries is shown. Reproduced from Rao PS, *Indian J Pediatr* 2015; 82:1147–1156 [36].

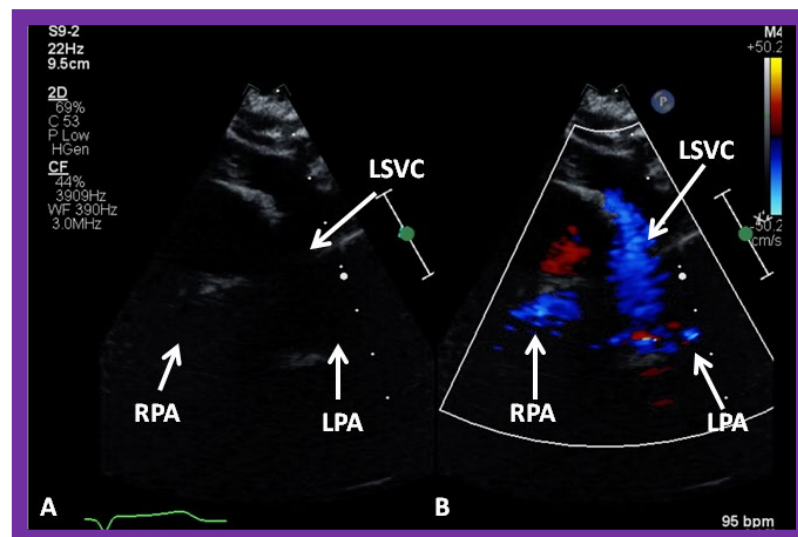


Figure 30. (A,B) Selected video frames from suprasternal notch view demonstrating left sided bidirectional Glenn shunt. In (A), the right (RPA) and left (LPA) pulmonary arteries are faintly seen by 2D. On color Doppler study, the visualization is slightly better (B). LSVC, left superior vena cava.

5.4. Echocardiographic Evaluation of Interstage Issues

Interstage mortality has been reported to occur in 5 to 15% of patients [50,51]. While the focus of these studies was on hypoplastic left heart syndrome, these principles are equally applicable to TA [36–38,52]. Interstage mortality occurs more often between Stages I and II than between Stages II and III. The causes of interstage mortality are restrictive atrial communication, obstruction of the aortic arch, distortion/stenosis of the pulmonary arteries, atrio–ventricular valve insufficiency, shunt blockage, and intercurrent illnesses [50–52]. Echo-Doppler studies are useful in detecting these abnormalities and should be routinely used to identify these issues so that they can be effectively addressed with medical, transcatheter and/or surgical methods, as deemed appropriate for a given clinical scenario and, thus, avoid or reduce interstage mortality.

5.4.1. Restrictive Inter-Atrial Communication

The adequacy of ASD/PFO in decompressing the RA should be evaluated; the presence of a wide open atrial defect with nonturbulent (laminar) flow across the atrial septum (Figure 18) should be demonstrated. It should be noted, however, that inter-atrial obstruction is more common in patients with hypoplastic syndrome, and its variants, than in subjects with TA. If 2D narrowing along with turbulent and/or high Doppler velocity across the PFO is seen, appropriate transcatheter or surgical relief [38,47] should be provided.

5.4.2. Obstruction of the Aortic Arch

Coarctation of the aorta is particularly common in Type II (transposition of the great arteries) patients; if present, it is usually dealt with at the time of initial palliation in the neonatal period. It is possible that coarctation was missed at the time of initial presentation or it may have developed subsequently. Alternatively, recoarctation may have developed following prior surgery or balloon angioplasty. Echo studies should be scrutinized to demonstrate the patency of the descending aorta (Figure 31) and, if coarctation is demonstrated (Figure 32; Figure 33), it should be treated either by balloon angioplasty or surgery, as deemed appropriate [38].

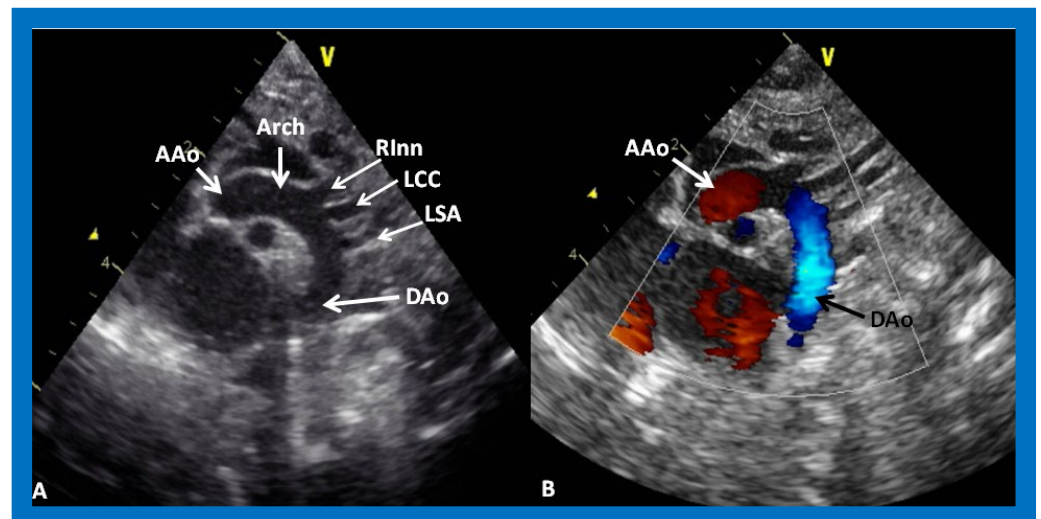


Figure 31. (A) Suprasternal notch view of a normal aortic arch (Arch) demonstrating the ascending aorta (AAo), aortic arch (Arch) and descending aorta (DAo). Note the origin of the right innominate (RIIn), left common carotid (LCC) and left subclavian (LSA) arteries, arising from the aortic arch. (B) The same view with color Doppler imaging, showing red flow in the AAo and blue flow in the DAo. Reproduced from Reference [53].

5.4.3. Branch Pulmonary Artery Abnormalities

Distortion or stenosis of the branch PAs may be secondary to palliative procedures performed at the time of initial presentation or may have developed spontaneously in the innate branch PAs. The careful 2D and Doppler interrogation of PAs should be undertaken to detect significant stenosis (Figure 34) or hypoplasia (Figure 35) and, if present, balloon angioplasty, stent implantation or surgery as deemed appropriate should be undertaken [38].

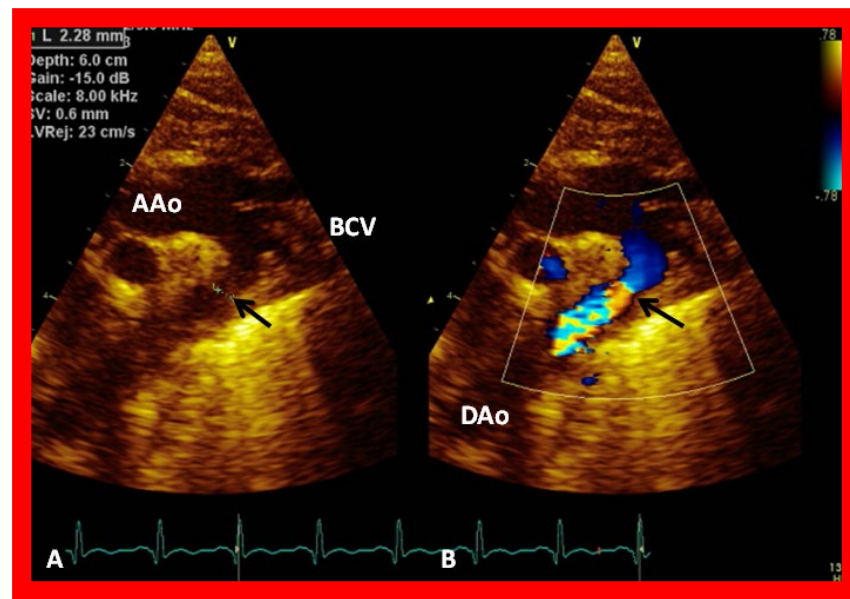


Figure 32. (A) Suprasternal notch view of the aortic arch (Arch) in a patient with aortic coarctation (arrow) in 2D (A) and color flow mapping (B), demonstrating turbulence at the site of coarctation (arrow). AAO, ascending aorta; BCV, brachiocephalic vessels; DAo, descending aorta. Reproduced from Reference [53].

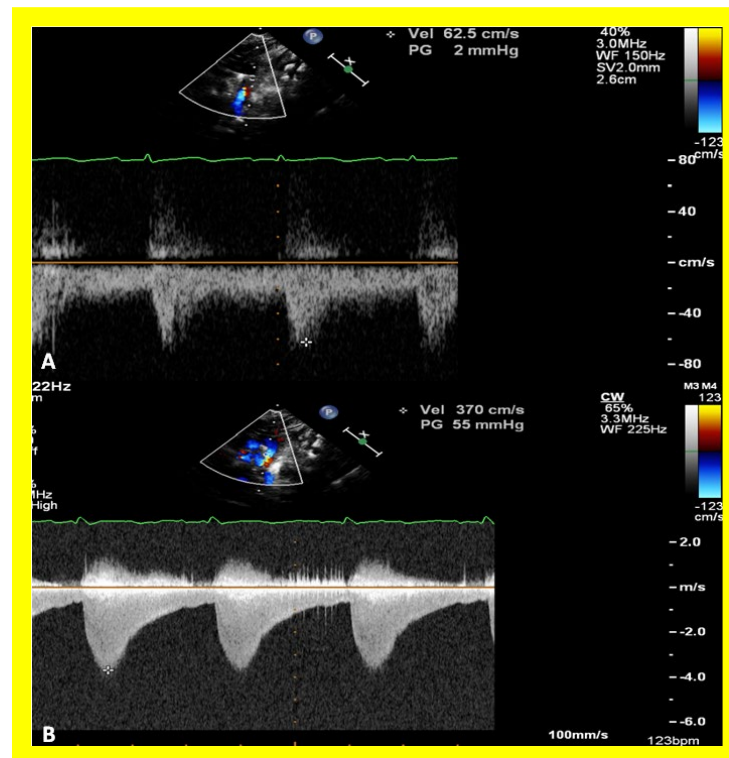


Figure 33. A Doppler interrogation of the aortic arch reveals a jump in the peak flow velocity from the proximal segment (A) to the segment distal to the coarctation (B). Continuous wave Doppler interrogation across the stenotic segment (B) shows high velocity (~ 4 m/s) with diastolic extension of the Doppler flow signal, suggesting that the coarctation is severe. Reproduced from Reference [53].

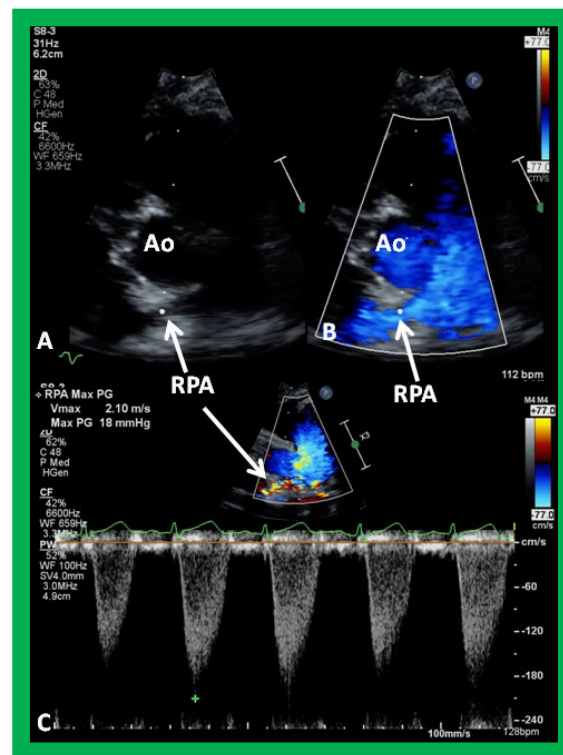


Figure 34. Selected video frames from parasternal short axis view demonstrating stenosis of the right pulmonary artery (RPA) by two dimensional (A) and color (B) and pulsed (C) Doppler imaging. Doppler calculated gradient was 18 mmHg (C). Ao, aorta.

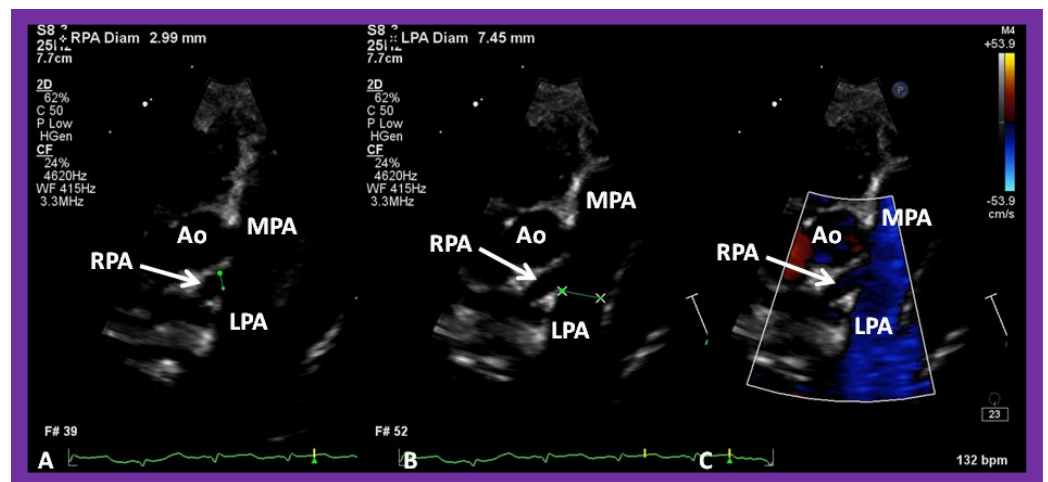


Figure 35. Selected video frames from parasternal short axis view demonstrating hypoplasia of the right pulmonary artery (RPA) in two dimensional (A,B) and color flow (C) images. The measurements of the RPA (A) and left pulmonary artery (LPA) (B) are shown. Ao, aorta; MPA, main pulmonary artery.

5.4.4. Mitral Valve Insufficiency

Mitral valve insufficiency (Figure 36) may develop during follow up and is routinely screened for during echo-Doppler studies. It may be either due to marked dilatation of the LV or secondary to a defect in the valve mechanism. If present, treatment with afterload reducing agents or surgical therapy (valvuloplasty/valve replacement) should be undertaken, as appropriate.

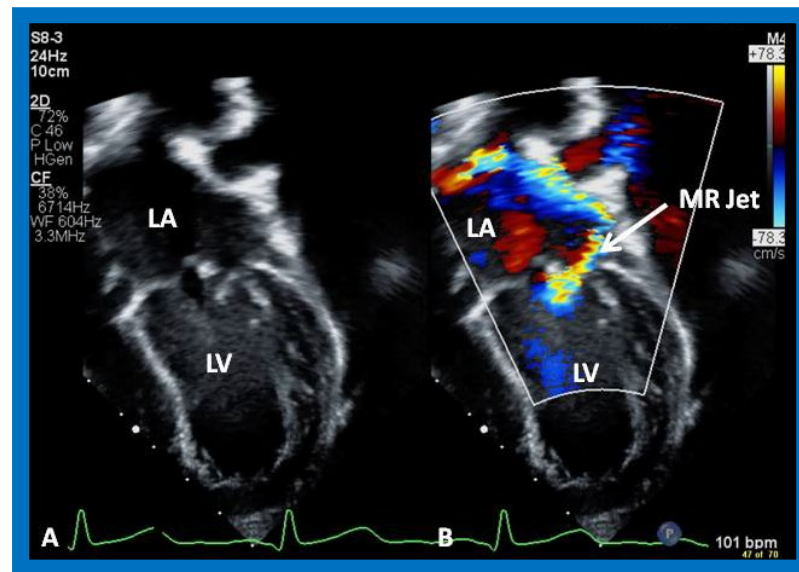


Figure 36. Selected video frames from apical four chamber view demonstrating dilated left atrium (LA) and left ventricle (LV) (A,B). Note the mitral insufficiency jet (MR Jet) in (B).

5.4.5. Shunt Blockage

Blockage of the aorto–pulmonary shunts may develop during follow up, which may either be complete or partial. Patients with complete blockage, usually due to thrombus formation, typically present with severe cyanosis and respiratory distress. Inability to demonstrate the shunt by color Doppler interrogation in a patient in whom a shunt was demonstrated in prior studies suggests complete shunt blockage. In patients who develop partial blockage, the obstruction may be either at the proximal anastomosis with the subclavian (or innominate) artery or aortic arch, at the distal anastomosis at the entry into the PA, or, rarely, somewhere in between (due to kinking). While these obstructive lesions are easily demonstrable on angiography (Figure 37), these narrowings are somewhat difficult to image by 2D. However, color flow disturbance along with high Doppler flow velocities at the site of obstruction suggest obstruction. Thrombolytic recanalization, transcatheter stent implantation, the surgical revision of the shunt, or bidirectional Glenn may be performed, depending upon the clinical scenario and institutional preference [38].

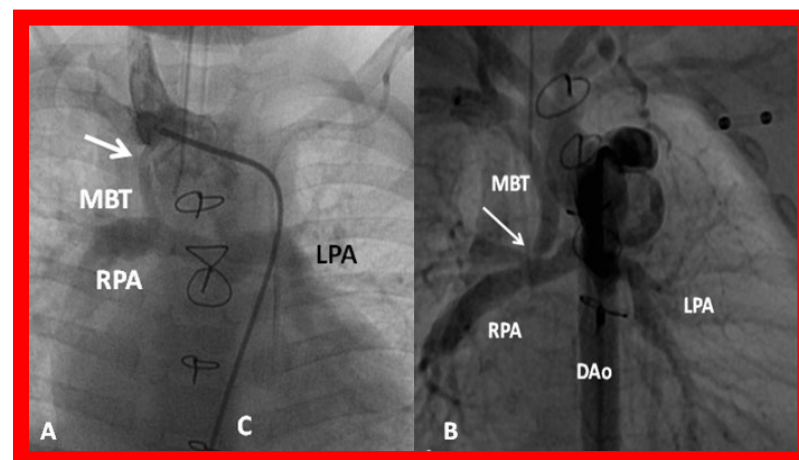


Figure 37. (A) Selected cine frame in a postero–anterior view demonstrating narrowing (arrow) of a modified Blalock–Taussig (MBT) shunt at its junction with the right innominate artery. (B) Similar angiographic frame from a different patient showing narrowing of the MBT (arrow) at its entry into the right pulmonary artery (RPA). C, catheter; DAo, descending aorta; LPA, left pulmonary artery.

5.4.6. Interventricular Obstruction

In Type II (transposition of the great arteries) patients, the VSD may be small and obstructive at the time of initial presentation in the neonatal period, which is usually addressed by performing a DKS procedure along with the other palliative measures. An initially adequate sized VSD may become spontaneously smaller with time or following a PA banding procedure [15,16,21]. Keeping this in mind, echo-Doppler studies should image the VSD with regard to its 2D size and Doppler flow velocity across this region (Figures 11, 12 and 15). Small 2D size and/or increased Doppler flow velocity across this region are indicative of obstruction.

5.5. Echocardiographic Evaluation Following Completion of Fontan

Subsequent to completion of Fontan procedure, periodic clinical follow up along with echo-Doppler studies is generally recommended at 1, 6, and 12 months after the procedure and yearly thereafter [36–38]. The LV is usually normal in size with normal LV systolic function (Figure 38) because the pulmonary and systemic circulations are completely separated during the final phase of Fontan. However, some patients may have dilatation of the LV with or without diminished LV systolic function, secondary to prolonged exposure to volume overloading, significant mitral insufficiency, previously undetected myocardial damage due to multiple surgical procedures under cardio-pulmonary bypass, or a combination thereof.

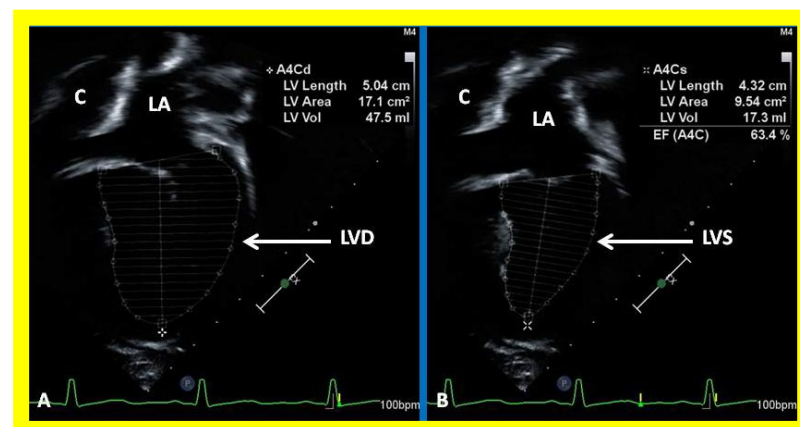


Figure 38. Selected video frames showing left ventricle (LV) in diastole (LVD) (A) and in systole (LVS) (B) demonstrating normal ejection fraction (EF) of 63.4%. C, conduit; LA, left atrium.

Post-Fontan echocardiographic anatomy is best displayed in apical four chamber views, as demonstrated in Figures 38–40. The remnants of the RA and the LA are seen (Figures 38–40). The remnants of atrial septum are not usually seen since the atrial septum is completely removed either during bidirectional Glenn or Fontan surgery. Unobstructed pathway allowing emptying of blood flow from the coronary sinus and thebesian veins is usually seen in an apical four chamber view (Figure 40).

The LA is usually normal in size (Figures 38–40) and empties into the LV; laminar flow across the mitral valve (Figure 41A) can be seen. Drainage of all four pulmonary veins into the LA may be demonstrated by color flow mapping in multiple echocardiographic views. The LV is either normal in size or slightly dilated. In type I patients with normally related great arteries, the LV outflow into the aorta is demonstrable on echo-Doppler with laminar, unobstructed flow with near normal (~1.0 m/s) Doppler flow velocity (Figures 41B and 42). The RV is small and hypoplastic (Figures 39 and 40). If the VSD has already spontaneously closed (Figure 40), the RV has no communication with any other structures since the connection with the PAs has been severed during bidirectional Glenn or Fontan procedures. If the VSD did not undergo spontaneous closure, the RV forms a cul-de-sac connection with the LV (Figures 39 and 43). In Type I patients with atresia of both tricuspid and pulmonary

valves (Type Ia), the hypertrophied RV may protrude into the LV outflow region (Figure 44). However, there is usually no evidence for obstruction across this region (Figure 45).

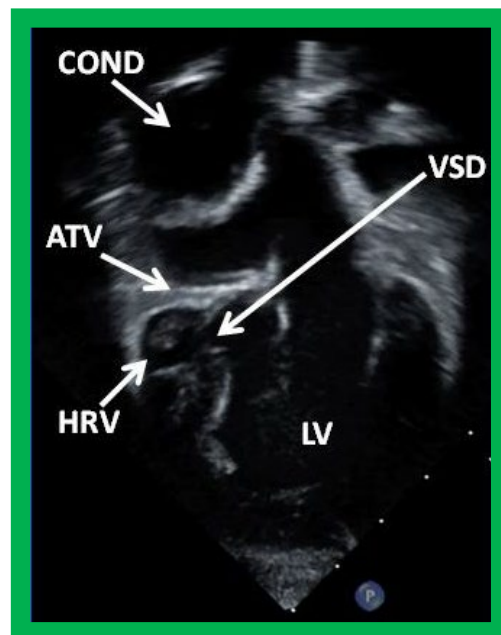


Figure 39. Selected video frame from an apical four-chamber view demonstrating the left ventricle (LV), hypoplastic right ventricle (HRV) with an atretic tricuspid valve (ATV) in a patient who had Fontan procedure. Cross-sectional view of the conduit (COND) is also shown. Note small ventricular septal defect (VSD) (long arrow).

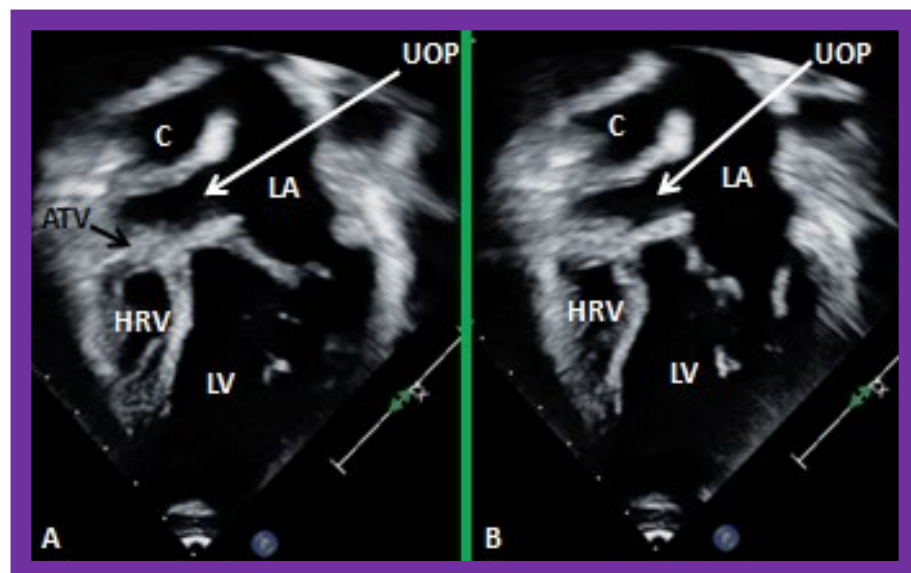


Figure 40. Selected video frames from apical four-chamber views demonstrating unobstructed pathway (UOP) (long arrow) between the right and left (LA) atria; the mitral valve is closed in (A) while it is open in (B). ATV, atretic tricuspid valve; C, conduit; HRV, hypoplastic right ventricle; LV, left ventricle.

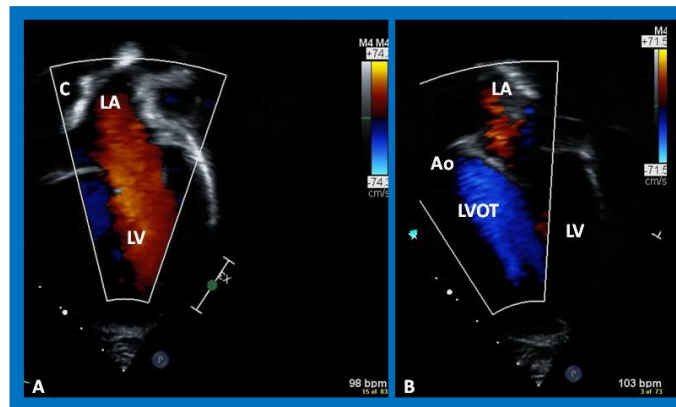


Figure 41. Selected video frames from an apical views demonstrating laminar flow from the left atrium (LA) to the left ventricle (LV) (A) and from the LV to aorta (Ao) (B). Note laminar flow in the LV outflow tract (LVOT) (B). Medial portion of the conduit (C) is seen in (A).

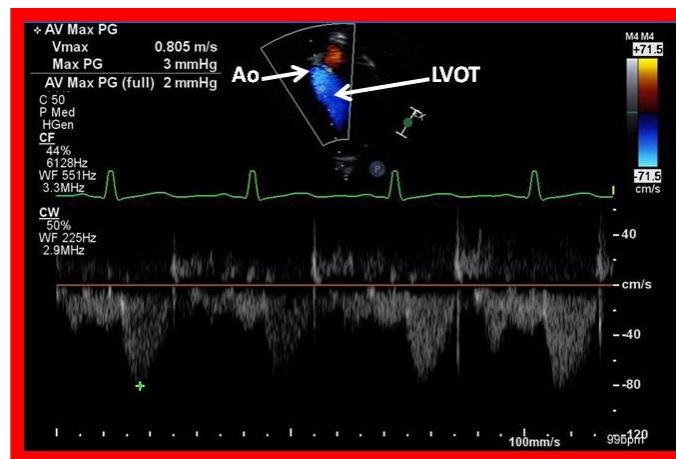


Figure 42. Selected video frames from an apical view demonstrating laminar flow from the left ventricle into the aorta (Ao). Note laminar flow in the LV outflow tract (LVOT) and low Doppler flow velocity (~ 0.8 m/s).

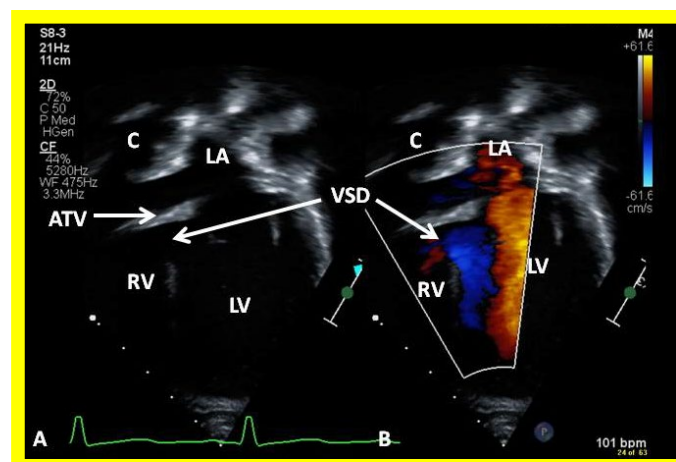


Figure 43. Selected video frames from apical views in two dimensional (A) and color flow imaging (B) modes demonstrating the right ventricle (RV) forming a cul-de-sac connection via a ventricular septal defect (VSD) with the left ventricle (LV). ATV, atretic tricuspid valve, C, conduit, LA, left atrium.

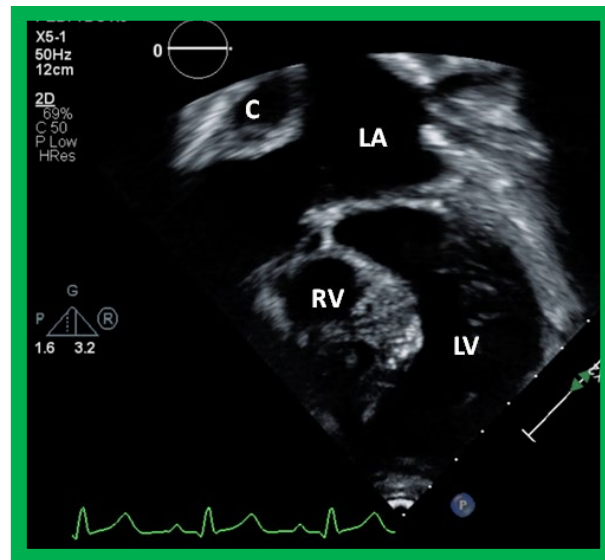


Figure 44. Selected video frame from an apical four-chamber view demonstrating the left ventricle (LV) and hypoplastic right ventricle (RV) in a patient who had a Fontan procedure. Note that the RV protrudes into the left ventricular (LV) outflow tract. Cross-sectional view of the conduit (C) is also shown. LA, left atrium.

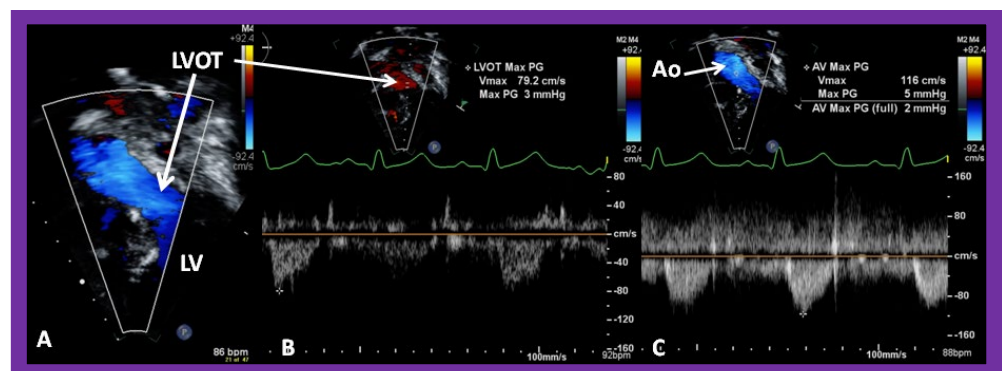


Figure 45. Selected video frame from an apical four-chamber view demonstrating that there is no evidence for left ventricular outflow tract (LVOT) obstruction in the patient shown in Figure 43. Note laminar flow across the LVOT in (A) and low Doppler flow velocities across the LVOT (B) and aorta (Ao) (C). LV, left ventricle.

In Type II patients with transposition of the great arteries, the LV outflow into the aorta is via the VSD and RV. If the VSD is large, the LV outflow is unobstructed (Figures 12 and 15). If the VSD is small and obstructive, the patient is likely to have had a DKS procedure earlier, bypassing the obstruction. Initially unobstructed VSD may become smaller with time [15,16] and, therefore, the echo studies should attempt to demonstrate obstruction across the VSD or the lack of it.

Cross-sectional views of the Fontan conduit were shown in Figures 38–40. Imaging of the conduit longitudinally is also possible (Figure 46) and laminar flow in the conduit (Figure 46B) is indicative of a nonobstructive conduit. The connection between the IVC and the conduit (Figures 47 and 48) can also be demonstrated by echo studies. Doppler interrogation demonstrating low flow velocities across this region (Figure 49) is indicative of nonobstructive IVC–conduit junction. Turbulent flow and high Doppler velocity across this region suggest obstruction; however, this is rarely seen.

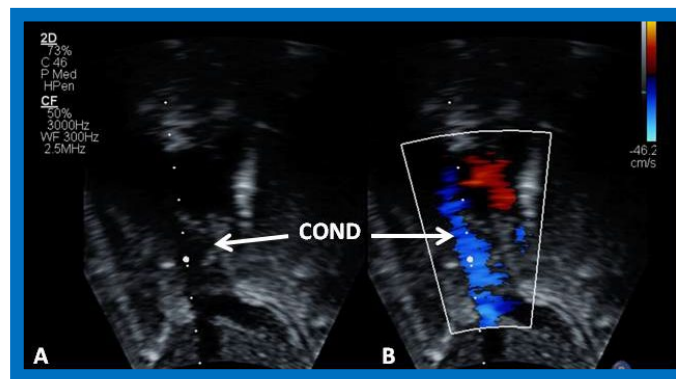


Figure 46. Selected video frame demonstrating wide open conduit (COND) by 2D (A) and color flow imaging (B). Note laminar flow in (B) indicating no obstruction.

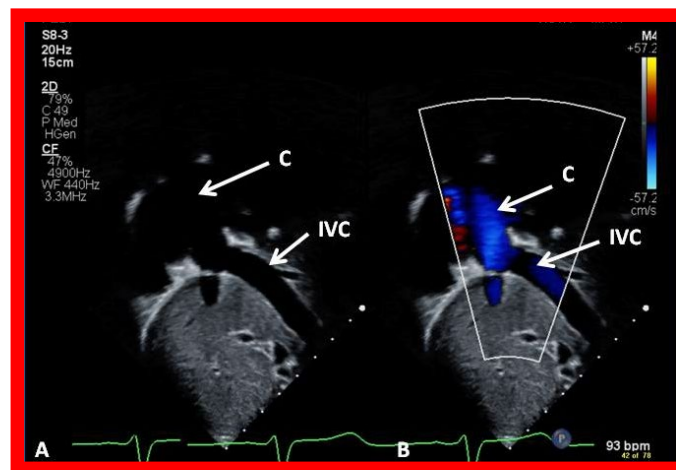


Figure 47. Selected video frames demonstrating connection between the inferior vena cava (IVC) and the conduit (C) by 2D (A) and color flow imaging (B); note that the IVC–C junction is wide open.

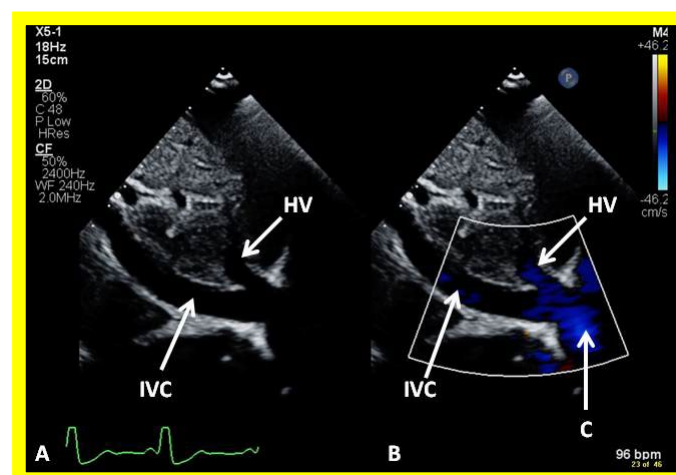


Figure 48. Selected video frames from subcostal view demonstrating connection between the inferior vena cava (IVC) and the conduit by 2D (A) and color flow imaging (B); note that the IVC to conduit (C) connection is wide open.

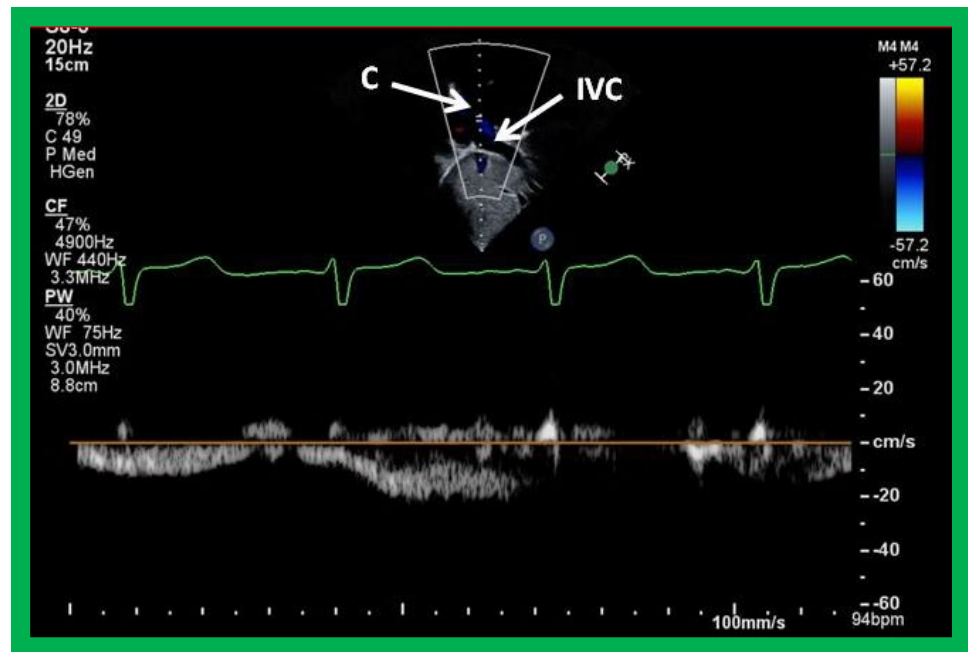


Figure 49. Selected video frame demonstrating low velocity flow between the inferior vena cava (IVC) and the conduit (C) shown in Figure 47, suggesting no evidence for obstruction.

Surgically created fenestrations (Figures 50–53) can also be demonstrated by color Doppler studies and the mean gradient across the fenestration (Figures 52 and 53) is helpful in determining the physiologic state; a mean gradient of 4 to 8 mmHg is considered adequate.

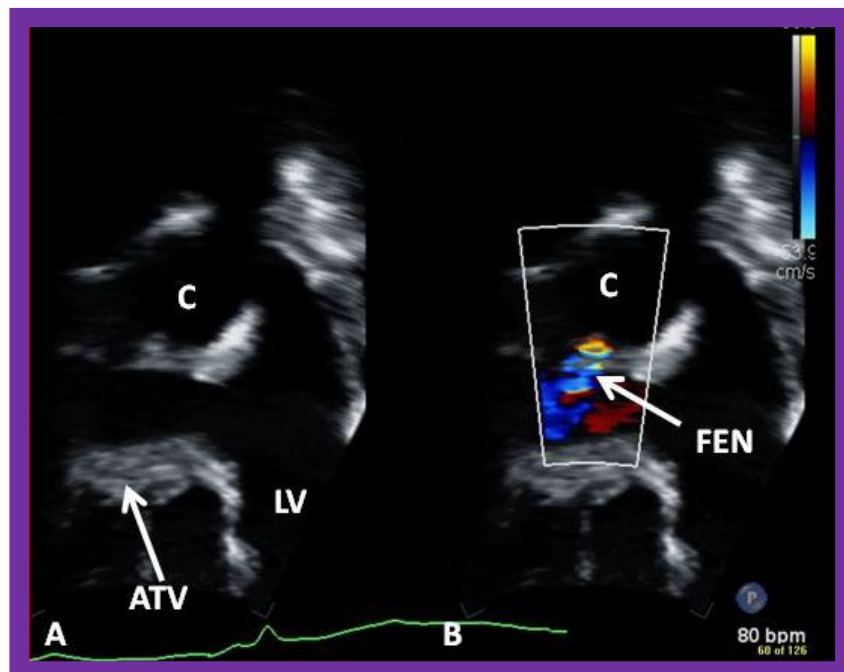


Figure 50. Selected video frames (A,B) from an apical four chamber view, similar to Figures 39 and 40, focusing on the conduit (C) (A) (left) and with color flow imaging (B) demonstrating fenestration (FEN). ATV, atretic tricuspid valve; LV, left ventricle.

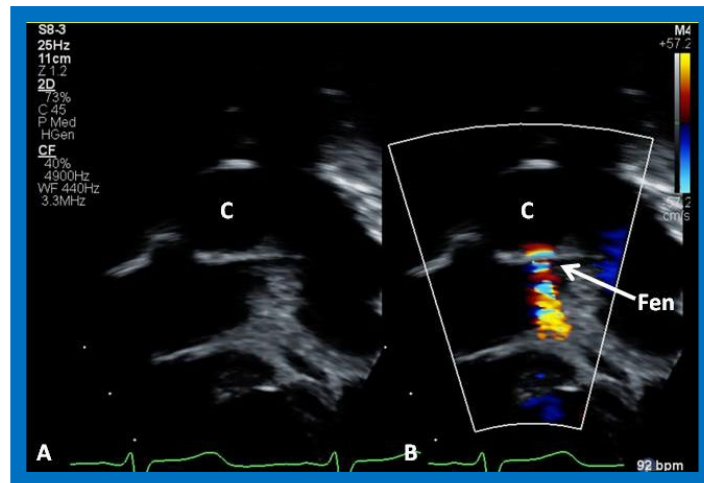


Figure 51. A magnified view of the fenestration (Fen), similar to Figure 50. C, conduit.

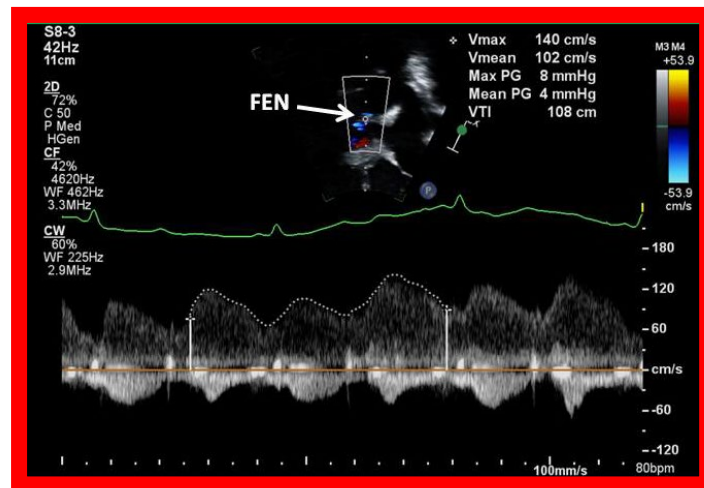


Figure 52. Selected video frame with Doppler sampling across the fenestration (Fen) demonstrating a mean gradient of 4 mmHg.

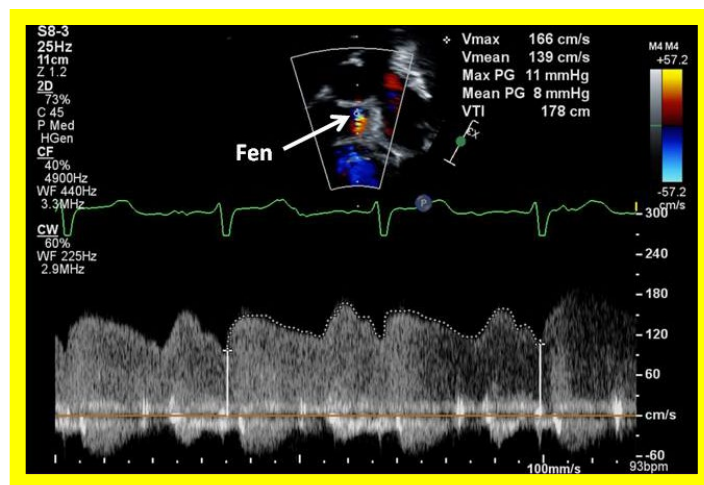


Figure 53. Selected video frame with Doppler sampling across the fenestration (Fen) demonstrating a mean gradient of 8 mmHg.

Angiographic counter part of the Fontan conduit with fenestration is shown, in Figure 54, to have better comprehension of the anatomy of the Fontan.

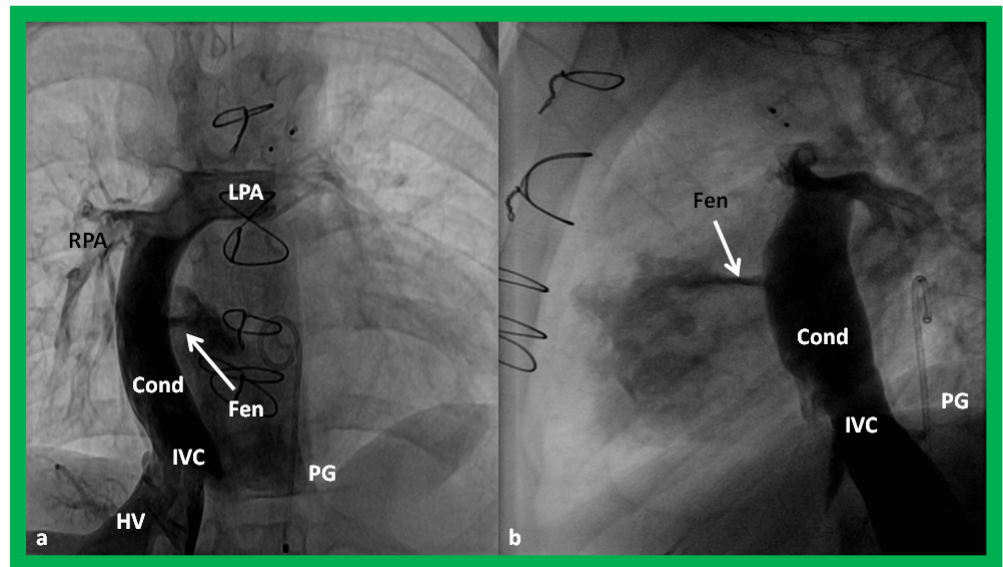


Figure 54. Selected cine frames in postero–anterior (a) and lateral (b) views, demonstrating Stage IIIA Fontan procedure diverting the inferior vena caval (IVC) flow into the pulmonary arteries via a nonvalve conduit (Cond). Flow across the fenestration (Fen) is shown by arrows in (a,b). HV, hepatic veins; LPA, left pulmonary artery; PG, pigtail catheter in the descending aorta; RPA, right pulmonary artery. Modified from Rao PS, *Indian J Pediatr*, 2015; 82:1147-56 [36].

The demonstration of the patency of a bidirectional Glenn component (Figures 25–27 and 30) of the Fontan is similar to that described in the section on “Echocardiographic Evaluation Following Bidirectional Glenn”. Color and CW Doppler interrogation across the SVC/PA/Conduit (Figure 55) is performed to ensure that there is no obstruction across this region.

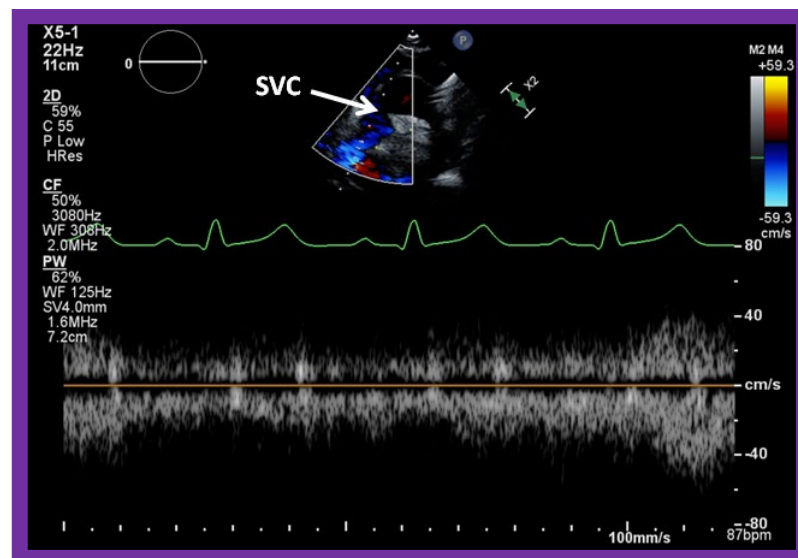


Figure 55. Selected video frames from suprasternal notch view, demonstrating low Doppler flow velocity across superior vena cava (SVC), bidirectional Glenn shunt and the conduit. Low Doppler flow velocity across the SVC, Glenn and the conduit indicates unobstructed Glenn component of the Fontan.

Following the device closure of the fenestration, the position of the device and lack of residual shunting (Figure 56) can usually be demonstrated on echo-Doppler studies. This is the counterpart of the appearance of device closure, seen during angiography (Figure 57).

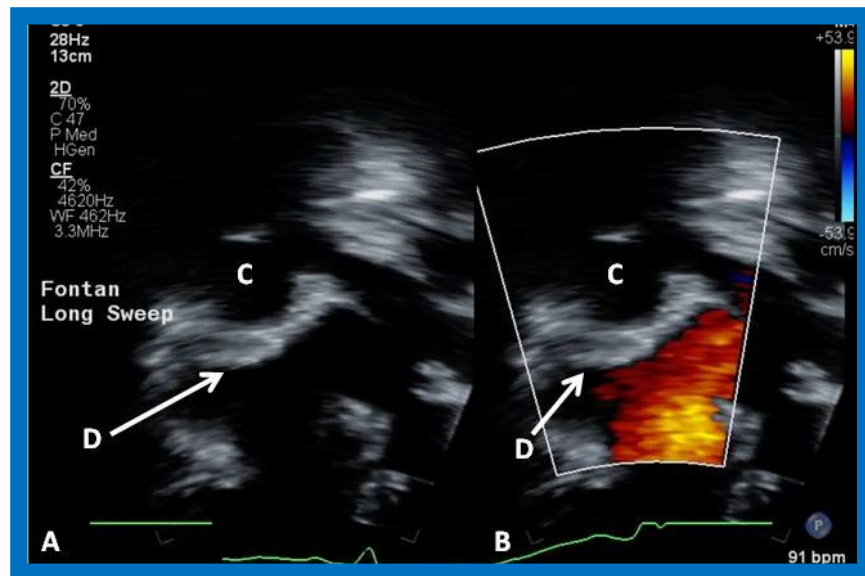


Figure 56. Selected video frames from apical four chamber view, demonstrating the position of the Amplatzer device (D) (arrows in (A,B)). No residual shunt is seen (B). C, conduit. See Figure 57 for the angiographic counterpart.

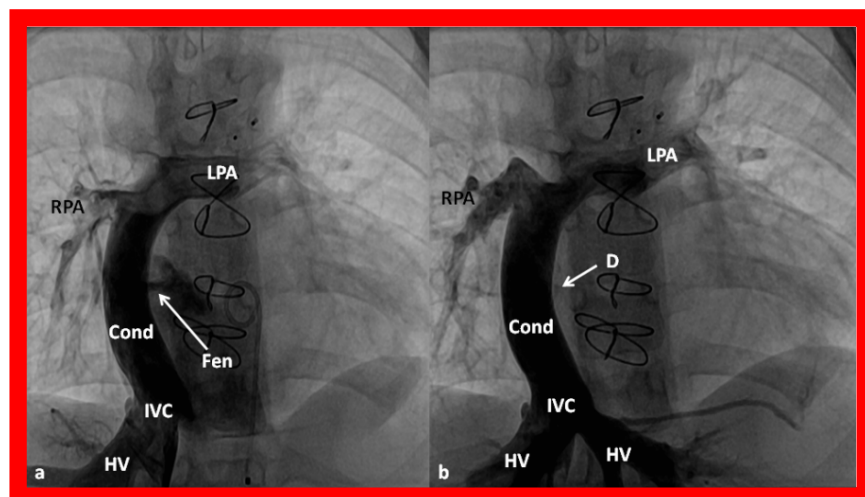


Figure 57. Selected cineangiographic frames in antero–posterior view, demonstrating Stage IIIA of the Fontan procedure: diverting the inferior vena caval (IVC) flow into the pulmonary arteries via a nonvalve conduit (Cond). Note the fenestration (Fen) shown by the arrow in (a) The Fen is closed with an Amplatzer device (D), shown by the arrow in (b) (Stage IIIB). HV, hepatic veins; LPA, left pulmonary artery; RPA, right pulmonary artery. Reproduced from Reference [36].

In addition to the complications listed in the section on “Echocardiographic Evaluation of Interstage Issues”, a number of other complications, namely, obstructed Fontan pathways, persistent shunts, thrombus formation (Figures 58 and 59), mitral insufficiency (Figure 36), systemic venous to pulmonary venous collateral vessels, and others [36–38], may occur during follow up after Fontan. The echocardiographer should be mindful of these complications and search for them, although not all of them can be detected by echocardiographic studies.

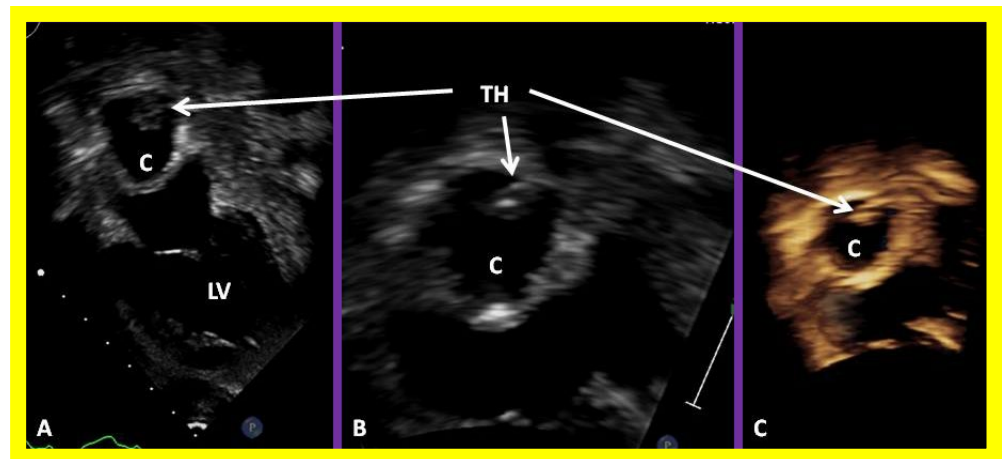


Figure 58. Selected video frames of 2D echocardiograms demonstrating a thrombus (TH) within the conduit (C) in a four chamber apical view (A) which was magnified in (B). 3D image is shown in (C). LV, left ventricle.

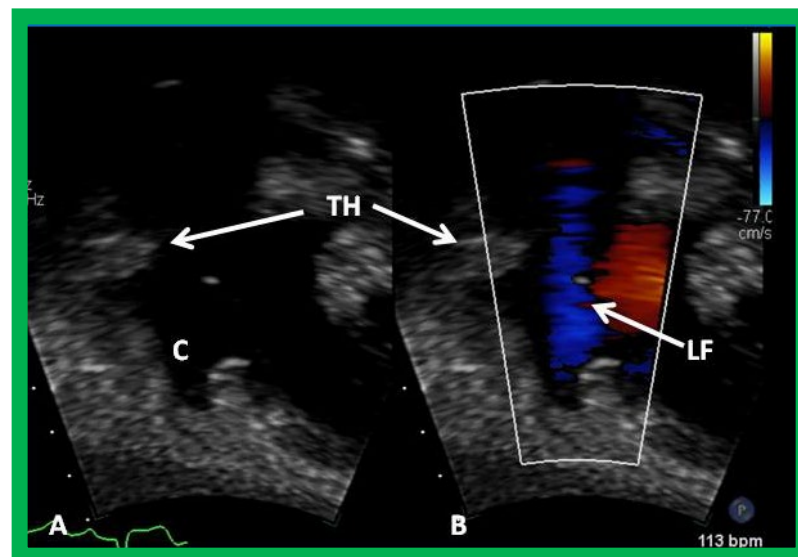


Figure 59. Selected video frames demonstrating wide open conduit (C) by 2D (A) and color flow imaging (B) despite the thrombus (TH). Laminar flow (LF) and pulsed and continuous wave Doppler interrogation (not shown) do not indicate obstruction.

While the echo-Doppler studies are helpful in ensuring adequacy of the Fontan procedure in most patients, poor echo windows may sometimes prevent adequate evaluation and in such situations, other imaging studies (MRI, CT), including angiography, may be required.

6. Summary and Conclusions

The major purpose of this review was to illustrate usefulness of echocardiography in the diagnosis and management of TA. TA is the third most common cyanotic CHD and accounts for almost 1.5% of all CHDs. TA is classified on the basis of the atretic tricuspid valve morphology and associated heart defects, such as great artery relationship and pulmonary outflow tract status. Initially, the anatomic features of TA were reviewed. The atretic tricuspid valve can easily be demonstrated on 2D echocardiography. Ventricular sizes and LV systolic function are first evaluated, followed by the delineation of great artery anatomy, the status of the pulmonary outflow tract, the demonstration of adequacy of ASD/PFO, the size of VSD, and other associated cardiac defects. Echo-Doppler studies are

also useful in evaluating the results of palliative procedures performed early in life, such as aorto–pulmonary shunts and the banding of the PA. Evaluation following bidirectional Glenn and Fontan completion, the assessment of potential causes of interstage mortality, and the identification of complications associated with all surgical procedures are also feasible by the echocardiographic studies. Examples of typical echocardiographic findings of most of the above scenarios were presented. It is concluded that echo-Doppler studies are valuable in the diagnosis and management of TA.

Funding: This research received no external funding.

Institutional Review Board Statement: Institutional Review Boards approved the respective studies.

Informed Consent Statement: Informed consent was obtained from all subjects involved in the respective studies.

Data Availability Statement: Not applicable.

Acknowledgments: The author wishes to acknowledge and thank the multiple sonographers, at several institutions where the author had the privilege to serve on their faculty, for their excellent work in securing the echocardiographic studies presented in this manuscript.

Conflicts of Interest: The author declares no conflict of interest.

References

1. Rao, P. A unified classification for tricuspid atresia. *Am. Heart J.* **1980**, *99*, 799–804. [[CrossRef](#)]
2. Rao, P.S. Terminology: Tricuspid atresia or univentricular heart? In *Tricuspid Atresia*, Mount Kisco; Futura Publishing Co.: New York, NY, USA, 1982; pp. 3–6.
3. Rao, P.S. Tricuspid atresia. In *Pediatric Cardiology: How It Has Evolved Over the Last 50 Years*; Cambridge Scholars Publishing: Newcastle, UK, 2020; pp. 24–69.
4. Rao, P.S. Demographic features of tricuspid atresia. In *Tricuspid Atresia*, 2nd ed.; Futura Publishing Co.: Mount Kisco, NY, USA, 1992; pp. 23–37.
5. Rowe, R.D.; Freedom, R.M.; Mehrizi, A.; Bloom, K.R. The neonate with congenital heart disease. In *Major Problems in Clinical Pediatrics*, 2nd ed.; WB Saunders: Philadelphia, PA, USA, 1981; pp. 456–479.
6. Vanpraagh, R.; Ando, M.; Dungan, W.T. Anatomic types of tricuspid atresia: Clinical and developmental implications (abstract). *Circulation* **1971**, *44*, 115.
7. Astley, R.; Oldham, J.S.; Parsons, C. Congenital Tricuspid Atresia. *Heart* **1953**, *15*, 287–297. [[CrossRef](#)] [[PubMed](#)]
8. Müller, H.; Fall, I. Über zwei fälle kongenitaler atreside des ostium venosum dextrum. *Jahrb. Kinderh. Phys. Erzieh.* **1906**, *63*, 235–249.
9. Edwards, J.E.; Burchell, H.B. Congenital Tricuspid Atresia: A Classification. *Med. Clin. N. Am.* **1949**, *33*, 1177–1196. [[CrossRef](#)]
10. Keith, J.D.; Rowe, R.D.; Vlad, P. Tricuspid atresia. In *Heart Disease in Infancy and Childhood*; Macmillan: New York, NY, USA, 1958; pp. 434–470.
11. Rao, P.S.; Alapati, S. Tricuspid atresia in the neonate. *Neonatal. Today* **2012**, *7*, 1–12.
12. Rao, P.S. Tricuspid atresia: Anatomy, imaging and natural history. In *Atlas of Heart Disease: Congenital Heart Disease*; Freedom, R., Ed.; Current Medicine: Philadelphia, PA, USA, 1997.
13. Rao, P.S. Classification of tricuspid atresia. In *Tricuspid Atresia*; Futura Publishing Co.: Mount Kisco, NY, USA, 1982; pp. 41–47.
14. Rao, P.S.; Sissman, N.J. Spontaneous Closure of Physiologically Advantageous Ventricular Septal Defects. *Circulation* **1971**, *43*, 83–90. [[CrossRef](#)] [[PubMed](#)]
15. Rao, P.S. Natural history of the ventricular septal defect in tricuspid atresia and its surgical implications. *Heart* **1977**, *39*, 276–288. [[CrossRef](#)] [[PubMed](#)]
16. Rao, P.S. Further observations on the spontaneous closure of physiologically advantageous ventricular septal defects in tricuspid atresia: Surgical implications. *Ann. Thorac. Surg.* **1983**, *35*, 121–131. [[CrossRef](#)]
17. Gallaher, M.E.; Fyler, D.C. Observations on Changing Hemodynamics in Tricuspid Atresia without Associated Transposition of the Great Vessels. *Circulation* **1967**, *35*, 381–388. [[CrossRef](#)]
18. Sauer, U.; Hall, D. Spontaneous Closure or Critical Decrease in Size of the Ventricular Septal Defect in Tricuspid Atresia with Normally Connected Great Arteries: Surgical Implications. *Herz* **1981**, 105–130. [[CrossRef](#)]
19. Rao, P.S. Physiologically advantageous ventricular septal defects (Letter). *Pediatr. Cardiol.* **1983**, *4*, 59–61. [[CrossRef](#)] [[PubMed](#)]
20. Rao, P. Natural history of ventricular septal defects in tricuspid atresia. In *Tricuspid Atresia*, 2nd ed.; Rao, P.S., Ed.; Futura Publishing Co.: Mount Kisco, NY, USA, 1992; pp. 261–293.

21. Rao, P.S. Subaortic obstruction after pulmonary artery banding in patients with tricuspid atresia and double-inlet left ventricle and ventriculoarterial discordance (Letter). *J. Am. Coll. Cardiol.* **1991**, *18*, 1585–1586. [[CrossRef](#)]
22. Rao, P.S.; Covitz, W.; Chopra, P.S. Principles of palliative management of patients with tricuspid atresia. In *Tricuspid Atresia*, 2nd ed.; Rao, P.S., Ed.; Futura Publishing Co.: Mount Kisco, NY, USA, 1992; pp. 297–320.
23. Rao, P.S. *Tricuspid Atresia*; Futura Publishing, Co.: Mount Kisco, NY, USA, 1982.
24. Covitz, W.; Rao, P.S. Non-invasive evaluation of patients with tricuspid atresia (Roentgenography, Echocardiography, and Nuclear Angiography). In *Tricuspid Atresia*; Rao, P.S., Ed.; Futura Publishing Co.: Mount Kisco, NY, USA, 1982; pp. 127–145.
25. Beppu, S.; Nimura, Y.; Tamai, M.; Nagata, S.; Matsuo, H.; Kawashima, Y.; Sakakibara, H. Two-dimensional echocardiography in the diagnosis of tricuspid atresia: Differentiation from other hypoplastic right heart syndromes and common atrioventricular canal. *Br. Heart J.* **1978**, *40*, 1174–1183. [[CrossRef](#)] [[PubMed](#)]
26. Seward, J.B.; Tajik, A.J. Current status of echocardiography in cyanotic congenital heart diseases. *Cardiovasc. Clin.* **1978**, *9*, 269–294.
27. Rao, P.S. Tricuspid atresia. In *Fetal and Neonatal Cardiology*; Long, W.A., Ed.; W.B. Saunders: Philadelphia, PA, USA, 1990; pp. 525–540.
28. Covitz, W.; Rao, P.S. Non-invasive evaluation of patients with tricuspid atresia (Roentgenography, echocardiography, and nuclear angiography). In *Tricuspid Atresia*, 2nd ed.; Rao, P.S., Ed.; Futura Publishing Co.: Mount Kisco, NY, USA, 1992; pp. 165–182.
29. Rao, P.S. Echocardiographic evaluation of neonates with suspected heart disease. In *Perinatal Cardiology: A Multidisciplinary Approach*; Rao, P.S., Vidyasagar, D., Eds.; Chapter 11; Cardiotext Publishing: Minneapolis, MN, USA, 2015.
30. Rao, P.S. Atrioventricular canal mimicking tricuspid atresia: Echocardiographic and angiographic features. *Heart* **1987**, *58*, 409–412. [[CrossRef](#)]
31. Rao, P.S.; Levy, J.; Nikicicz, E.; Gilbert-Barness, E.F. Tricuspid atresia: Association with persistent truncus arteriosus—A review. *Am. Heart J.* **1991**, *122*, 829–835. [[CrossRef](#)]
32. Fontan, F.; Baudet, E. Surgical repair of tricuspid atresia. *Thorax* **1971**, *26*, 240–248. [[CrossRef](#)]
33. Kreutzer, G.; Bono, H.; Galindez, E. Una operacion para la correccion de la atresia tricuspidea. In Proceedings of the Ninth Argentinean Congress of Cardiology, Buenos Aires, Argentina, 31 October–6 November 1971.
34. Chopra, P.S.; Rao, P. Corrective surgery for tricuspid atresia: Which modification of Fontan-Kreutzer procedure should be used? A review. *Am. Heart J.* **1992**, *123*, 758–767. [[CrossRef](#)]
35. Rao, P.S.; Chopra, P.S. Modification of Fontan-Kreutzer procedures for tricuspid atresia: Can a choice be made? In *Tricuspid Atresia*, 2nd ed.; Rao, P.S., Ed.; Futura Publishing Co.: Mount Kisco, NY, USA, 1992; pp. 361–375.
36. Rao, P.S. Fontan operation: Indications, short and long term outcomes. *Indian J. Pediatr.* **2015**, *82*, 1147–1156. [[CrossRef](#)]
37. Rao, P.S. Fontan Operation: A Comprehensive Review. *Adv. Complex Valv. Dis.* **2021**. [[CrossRef](#)]
38. Rao, P. Single Ventricle—A Comprehensive Review. *Children* **2021**, *8*, 441. [[CrossRef](#)] [[PubMed](#)]
39. De Leval, M.R.; Kilner, P.; Gewilling, M.; Bull, C.; McGoon, D.C. Total cavopulmonary connection: A logical alternative to atriopulmonary connection for complex Fontan operation. *J. Thorac. Cardiovasc. Surg.* **1988**, *96*, 682–695. [[CrossRef](#)]
40. Hopkins, R.A.; Armstrong, B.E.; Serwer, G.A.; Peterson, R.J.; Oldham, H.N. Physiological rationale for a bidirectional cavopulmonary shunt. A versatile complement to the Fontan principle. *J. Thorac. Cardiovasc. Surg.* **1985**, *90*, 391–398. [[CrossRef](#)]
41. Kumar, S.P.; Rubinstein, C.S.; Simsic, J.M.; Taylor, A.B.; Saul, J.P.; Bradley, S.M. Lateral tunnel versus extracardiac conduit fontan procedure: A concurrent comparison. *Ann. Thorac. Surg.* **2003**, *76*, 1389–1397. [[CrossRef](#)]
42. Marcelletti, C.; Corno, A.; Giannico, S.; Marino, B. Inferior vena cava-pulmonary artery extracardiac conduit. A new form of right heart bypass. *J. Thorac. Cardiovasc. Surg.* **1990**, *100*, 313–314. [[CrossRef](#)]
43. Bridges, N.D.; Lock, J.E.; Castaneda, A.R. Baffle fenestration with subsequent transcatheter closure: Modification of the Fontan operation for patients with increased risk. *Circulation* **1990**, *82*, 1681–1689. [[CrossRef](#)]
44. Laks, H.; Pearl, J.M.; Haas, G.S.; Drinkwater, D.C.; Milgalter, E.; Jarmakani, J.M.; Isabel-Jones, J.; George, B.L.; Williams, R.G. Partial Fontan: Advantages of an adjustable interatrial communication. *Ann. Thorac. Surg.* **1991**, *52*, 1084–1095. [[CrossRef](#)]
45. De Leval, M.R.; McKay, R.; Jones, M.; Stark, J.; Macartney, F.J. Modified Blalock-Taussig shunt: Use of subclavian orifice as a flow regulator in prosthetic systemic-pulmonary artery shunts. *J. Thorac. Cardiovasc. Surg.* **1981**, *18*, 112–119. [[CrossRef](#)]
46. Muller, W.H.; Danimann, J.F. The treatment of certain congenital malformations of the heart by the creation of pulmonic stenosis to reduce pulmonary hypertension and excessive pulmonary blood flow; a preliminary report. *Surg. Gynecol. Obstet.* **1952**, *95*, 213–219.
47. Rashkind, W.; Waldhausen, J.; Miller, W.; Friedman, S. Palliative treatment of tricuspid atresia: Combined balloon atrial septostomy and surgical alteration of pulmonary blood flow. *J. Thorac. Cardiovasc. Surg.* **1969**, *57*, 812–818. [[CrossRef](#)]
48. Rao, P.S. Role of interventional cardiology in neonates: Part I. Non-surgical atrial septostomy. *Congenit. Cardiol. Today* **2007**, *5*, 1–12.
49. Rao, P.S. Neonatal catheter interventions. In *Cardiac Catheterization and Imaging (From Pediatrics to Geriatrics)*; Vijayalakshmi, I.B., Ed.; Jaypee Publications: New Delhi, India, 2015; pp. 388–432.
50. Bartram, U.; Grunenfelder, J.; Van Praagh, R. Causes of death after the modified Norwood procedure: A study of 122 postmortem cases. *Ann. Thorac. Surg.* **1997**, *64*, 1795–1802. [[CrossRef](#)]

-
51. Tweddell, J.S.; Hoffman, G.M.; A Mussatto, K.; Fedderly, R.T.; Berger, S.; Jaquiss, R.D.B.; Ghanayem, N.S.; Frisbee, S.J.; Litwin, S.B. Improved survival of patients undergoing palliation of hypoplastic left heart syndrome: Lessons learned from 115 consecutive patients. *Circulation* **2002**, *106*, 1–82. [[CrossRef](#)]
 52. Yates, M.C.; Rao, P.S. Pediatric cardiac emergencies. *Emerg. Med.* **2013**, *3*, 164.
 53. Rao, P.S. Coarctation of the aorta. In *A Multidisciplinary Approach to Perinatal Cardiology*; Rao, P., Vidyasagar, D., Eds.; Cambridge Scholars Publishing: New Castle, Tyne, UK, 2021; pp. 518–540. Volume 2, ISBN 978-1-5275-6744-3.